Inorganic Chemistry

Article

pubs.acs.org/IC

Synthesis, Structure, and Optical Properties of Pt(II) and Pd(II) Complexes with Oxazolyl- and Pyridyl-Functionalized DPPM-Type Ligands: A Combined Experimental and Theoretical Study

Shuanming Zhang,[†] Roberto Pattacini,[†] Pierre Braunstein,*[,†] Luisa De Cola,*[,‡] Edward Plummer,[‡] Matteo Mauro,[‡,§] Christophe Gourlaouen,[∥] and Chantal Daniel*[,∥]

[†]Laboratoire de Chimie de Coordination, Institut de Chimie (UMR 7177 CNRS/UdS), Université de Strasbourg, 4 rue Blaise Pascal, F-67081 Strasbourg, France

[‡]Laboratoire de Chimie et des Biomatériaux Supramoléculaires ISIS, 8 rue Gaspard Monge, BP 70028, F-67083 Strasbourg Cedex, France

[§]University of Strasbourg Institute for Advanced Study (USIAS), 5 allée du Général Rouvillois, 67083 Strasbourg, France

[∥]Laboratoire de Chimie Quantique, Institut de Chimie (UMR 7177 CNRS/UdS), Université de Strasbourg, 1 rue Blaise Pascal, BP 296/R8, F-67008 Strasbourg Cedex, France

Supporting Information

ABSTRACT: New square-planar complexes $[Pt(\mathbf{1}_{-H})_2]$ (**2a**) [$\mathbf{1}_{-H}$ = (oxazolin-2-yl)bis(diphenylphosphino)methanide] and $[Pd(\mathbf{1}_{-H})_2]$ (**2b**), of general formula $[M\{(Ph_2P)_2C{-}{-}{-}C{-}{-}{-}NCH_2CH_2O\}_2]$ (M = Pt, **2a**; M = Pd, **2b**), result from deprotonation of 2-{bis(diphenylphosphino)methyl}oxazoline (**1**) at the PCHP site. The new, functionalized dppm-type ligand 4-{bis(diphenylphosphino)methyl}pyridine, $(Ph_2P)_2CH(4\text{-}C_5H_4N)$ (**4**), was prepared by double lithiation and phosphorylation of 4-picoline. In the presence of NEt_3, the reactions of 2 equiv of **4** with $[PtCl_2(NCPh)_2]$ and $[Pd(acac)_2]$ (acac = acetylacetonate) afforded $[Pt(\mathbf{4}_{-H})_2]$ (**5a**) [$\mathbf{4}_{-H}$ = bis(diphenylphosphino)(pyridin-4-yl)methanide] and $[Pd(\mathbf{4}_{-H})_2]$ (**5b**), of general formula $[M\{(Ph_2P)_2C(4\text{-}C_5H_4N)\}_2]$ (M = Pt, **5a**; M = Pd, **5b**), respectively. In the absence of base, the reactions of 2 equiv of **4** with $[PtCl_2(NCPh)_2]$ and $[PdCl_2(NCPh)_2]$ afforded (**5a**·2HCl) (**6a**) and (**5b**·2HCl) (**6b**), respectively, in which the PCHP proton of **4** has migrated from carbon to nitrogen to give a pyridinium derivative of general formula $[M\{(Ph_2P)_2C(4\text{-}C_5H_4NH)\}_2]Cl_2$ (M = Pt, **6a**; M = Pd, **6b**). The complexes **3a**, **5a**·2MeOH, and **6b**·$4CH_2Cl_2$ have been structurally characterized by X-ray diffraction. The absorption/emission properties of the Pt(II) complexes **2a** and **5a** and the Pd(II) complexes **2b** and **5b** have been investigated by UV−vis spectroscopy and theoretical analysis based on density functional theory. The UV−vis absorption spectra of the neutral complexes recorded in dilute *N*,*N*′-dimethylformamide solutions are dominated by intense spin-allowed intraligand transitions in the region below 350 nm. The complexes exhibit charge-transfer bands between 350 and 500 nm. The experimental and theoretical absorption spectra agree qualitatively and point to two low-lying ligand-to-metal charge transfer states that contribute to the bands observed between 350 and 500 nm. The complexes are emissive in frozen solutions at 77 K, in the pure solid state, and when doped into films of poly(methyl methacrylate) but are nonemissive in solution. A red shift is observed when Pt(II) is replaced by Pd(II).

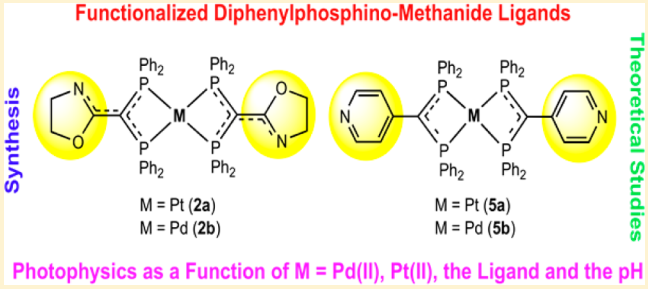

INTRODUCTION

The synthesis and study of heterotopic ligands bearing phosphorus and nitrogen donor atoms represent increasingly active fields of research because of the sometimes unexpected structural features associated with their metal complexes and the often unique properties of the latter, in particular for stoichiometric or catalytic transformations, that originate from the different stereoelectronic properties of the P and N donor groups.[1,2] Because of our combined interest in the synthesis and applications of such P,N ligands in coordination chemistry and catalysis[2−4] and in short-bite diphosphine ligands such as bis(diphenylphosphino)methane, $Ph_2PCH_2PPh_2$ (dppm), bis(diphenylphosphino)amine, $Ph_2PNHPPh_2$ (dppa), and their derivatives, which are well-known for their ability to stabilize di- or polynuclear complexes and clusters[5] and allow, e.g., their anchoring inside nanoporous membranes,[6] we decided to introduce an oxazoline moiety as a substituent on the PCP carbon of the dppm ligand.[3] The coordination behavior of 2-{bis(diphenylphosphino)-methyl}oxazoline, $(Ph_2P)_2CHC{=}NCH_2CH_2O$ (**1**) (Scheme 1), has barely been examined.[4]

Received: July 4, 2014
Published: November 24, 2014

Scheme 1. Ligands 2-{Bis(diphenylphosphino)-methyl}oxazoline (1) and 2-{Bis(diphenylphosphino)-methyl}pyridine

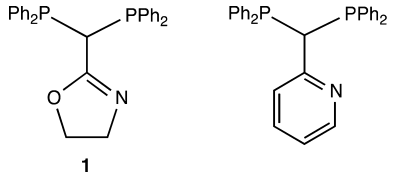

1

Comparative studies performed with 2-{bis(diphenylphosphino)methyl}pyridine, $(Ph_2P)_2CH(2\text{-}C_5H_4N)$, could shed light on the possible influence of the different basicities of the N-heterocycles on the chemistry and properties of their metal complexes. Various coordination modes have been evidenced for this ligand, with κ^2-*P,P*, κ^2-*P,N*, or κ^3-*N,P,P* bonding in mononuclear complexes[7,8] and μ-κ^2-*P,P* or μ-κ^1-*P*:κ^2-*P,N* bonding modes in dinuclear complexes.[8,9] However, coordination of the deprotonated form of 2-{bis(diphenylphosphino)-methyl}pyridine has rarely been described.[7] Interestingly, to the best of our knowledge, no reactions involving migration of PC*H*P or C*PPh*$_2$ to the pyridine nitrogen atom have been reported for this ligand (Scheme 2), in contrast to reactions

Scheme 2. PC*H*P and C*PPh*$_2$ Migration Reactions for 2-{Bis(diphenylphosphino)methyl}pyridine

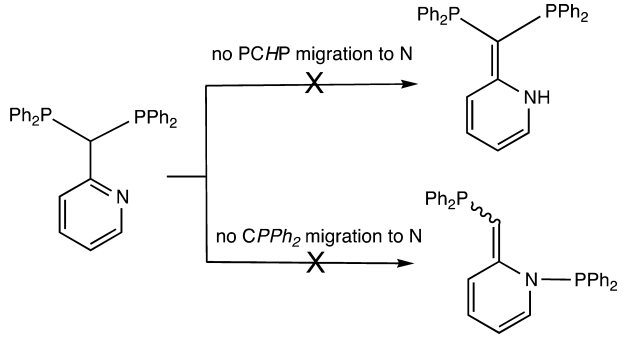

observed with the analogous oxazoline-containing diphosphine ligand.[3] It has been suggested that the absence of such migration reactions originates from the aromatic character of the pyridine moiety and the insufficient basicity of its nitrogen atom.[3]

It is well-established that many d^8 Pt(II) complexes display interesting luminescence properties, which have found applications in, e.g., sensing of volatile organic molecules[10] and in organic light-emitting diodes (OLEDs).[11] They usually display higher-energy excited states, better emission quantum yields, and longer lifetimes than their Pd(II) analogues as a result of strong spin−orbit coupling.[12] Numerous luminescent Pt(II) tertiary phosphine complexes have been reported in the literature, which generally display increased quantum yields and emission lifetimes due to the strong ligand field exerted by the phosphine ligands, which increases the d−d transition energies.[13] The dppm ligand has been widely used in this context.[14]

With the objectives to take advantage of the bonding properties of the short-bite diphosphines mentioned above and to enhance their interactions with metal centers, we prepared Pt(II) and Pd(II) complexes featuring functionalized diphosphinomethanides derived from PCP-substituted dppm-type ligands by deprotonation of the PCHP hydrogen (Scheme 3, R^1 = generic neutral group). Several structurally characterized

Scheme 3. Preparation of Diphosphinomethanides from a dppm-Type Ligand (R^1 = Neutral Group)

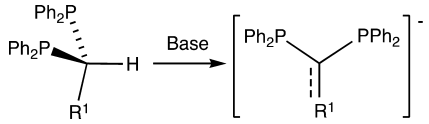

diphosphinomethanide Pd(II) and Pt(II) complexes have been reported, and the photophysical properties of, e.g., [Pd({2,2′:6′,2″-terpyridin-4′-yl}bis(diphenylphosphino)-methanide)$_2$] (Scheme 4) have been investigated.[15]

Scheme 4. Complex [Pd({2,2′:6′,2″-terpyridin-4′-yl}bis(diphenylphosphino)methanide)$_2$]

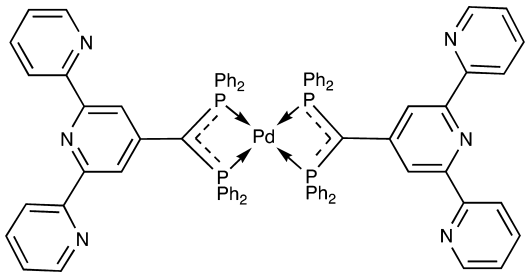

We recently reported that **1** (Scheme 1) readily reacts with Pt(II) and Pd(II) precursors in the presence of a base to afford the bis-*P,P*-chelated complexes [Pt($\mathbf{1}_{-H}$)$_2$] (**2a**) and [Pd($\mathbf{1}_{-H}$)$_2$] (**2b**), respectively (Scheme 5).[3] However, depending on the solvent in which the deprotonation of **1** was carried out, unexpected changes in the coordination modes of (oxazolin-2-yl)-bis(diphenylphosphino)methanide ($\mathbf{1}_{-H}$) were observed, as it can even exhibit both *P,P* and *P,N* chelating modes within the same complex (Scheme 6).[3] The bonding parameters of the ligand $\mathbf{1}_{-H}$ are consistent with the diphosphine and diphosphinomethanide limiting forms shown in Scheme 7.[3] For simplicity, in the following we shall represent the phosphorus−metal bonds involving this anionic ligand by simple lines.

The present study describes the synthesis, characterization (including by single-crystal X-ray diffraction), and reactivity of bis-*P,P*-chelated Pd(II) and Pt(II) complexes containing the new ligand 4-{bis(diphenylphosphino)methyl}pyridine and a detailed combined experimental and theoretical investigation of their luminescence properties.

RESULTS AND DISCUSSION

A. Synthesis and Characterization of the Metal Complexes. The neutral Pt(II) and Pd(II) complexes [Pt($\mathbf{1}_{-H}$)$_2$] (**2a**) and [Pd($\mathbf{1}_{-H}$)$_2$] (**2b**), in which two $\mathbf{1}_{-H}$ ligands bis-chelate the metal center through the phosphorus donors (Scheme 5),[3] were readily protonated in the solid state by HBF_4 (aqueous or as the Et_2O adduct) to give the cationic complexes [Pt(**1′**)$_2$]$(BF_4)_2$ (**3a**) [**1′** = 2-{bis(diphenylphosphino)methylene}oxazolidine] and [Pd(**1′**)$_2$]$(BF_4)_2$ (**3b**) (Scheme 8). The cationic complex $[Pt(\mathbf{1'})_2]^{2+}$ also forms upon reaction of **1** with $[PtCl_2(NCPh)_2]$ in MeCN or CH_2Cl_2.[3] In **3a** and **3b**, ligand **1′** has a protonated heterocyclic nitrogen (Scheme 9), in contrast to its tautomer **1**, which is the only form of the uncoordinated ligand that has been isolated and observed spectroscopically. The site of protonation in both **3a** and **3b** was clearly established by ^1H NMR spectroscopy (CD_3CN) with the appearance of NH resonances at

dx.doi.org/10.1021/ic501566u | Inorg. Chem. 2014, 53, 12739−12756

Scheme 5. Reaction of 2-{Bis(diphenylphosphino)methyl}oxazoline (1) with Pt(II) and Pd(II) Precursors To Give the Bis-*P,P*-chelated Complexes $[Pt(1_{-H})_2]$ (2a) and $[Pd(1_{-H})_2]$ (2b), Respectively

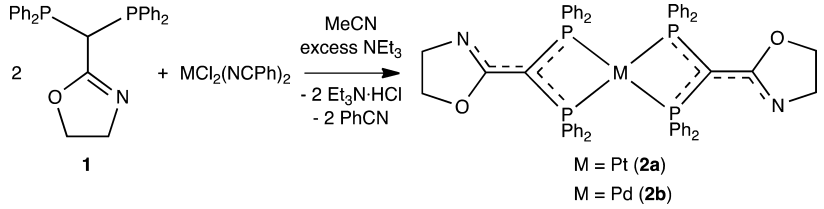

Scheme 6. *P,P*- and *P,N*-Chelating Modes of the Ligand 1_{-H} within the Same Complex

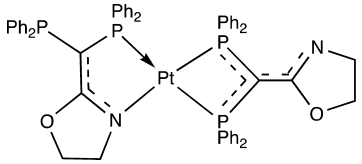

Scheme 7. Limiting Resonance Structures for the Ligand 1_{-H}

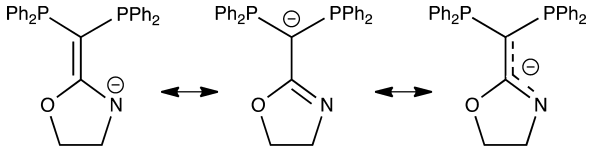

Scheme 8. Protonation of $[Pt(1_{-H})_2]$ (2a) and $[Pd(1_{-H})_2]$ (2b) in the Solid State To Give the Cationic Complexes $[Pt(1')_2](BF_4)_2$ (3a) [1′ = 2-{Bis(diphenylphosphino)methylene}oxazolidine] and $[Pd(1')_2](BF_4)_2$ (3b)

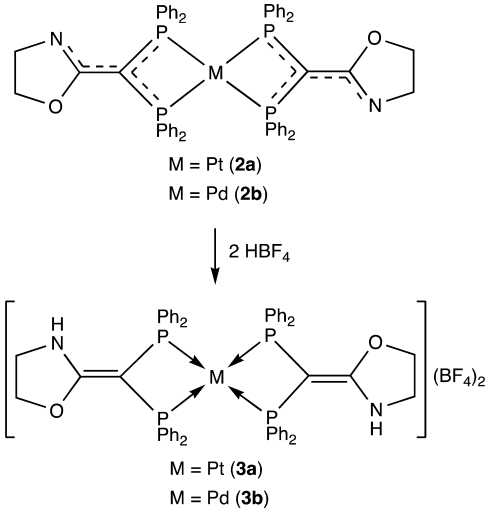

Scheme 9. Protonated Heterocyclic Nitrogen Ligand 1′ in 3a and 3b

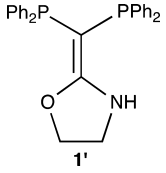

6.57 and 6.62 ppm, respectively. These signals disappear in CD_3OD solution as a result of H/D exchange.

The molecular structure of **3a** was determined by single-crystal X-ray diffraction methods (Figure 1). In the centrosymmetric structure of the cationic complex $[Pt(1')_2]^{2+}$ in **3a**, the metal center is bis-chelated by two $(Ph_2P)_2C{=}CN(H)CH_2CH_2O$ (**1′**) ligands (Scheme 9) through the phosphorus atoms. The square-planar coordination geometry around the metal center is rectangularly distorted [P1−Pt1−P2 = 72.01(3)° and P1−Pt1−$P2^i$ = 107.99(3)°]. Selected bond lengths in **3a** are compared with those in **2a** in Table 1. Only a slight elongation of the

Table 1. Selected Bond Distances (in Å) for Compounds 3a and 2a, Together with a Common Atom Numbering Scheme (Phenyl Groups Omitted)

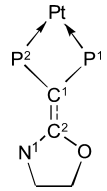

bond	3a	2a[a]
C1−P1	1.770(4)	1.751(2)
C1−P2	1.762(3)	1.745(3)
C1−C2	1.386(5)	1.432(3)
C2−N1	1.314(5)	1.299(3)

[a]Data from ref 3.

C2−N1 bond [1.314(5) Å] is observed in **3a** compared with **2a** [1.299(3) Å], while the C1−C2 bond is significantly shorter in **3a** [1.386(5) Å] than in **2a** [1.432(3) Å]. The C−P bonds in **3a** [1.770(4) and 1.762(3) Å] are slightly longer than those in **2a** [1.751(2) and 1.745(3) Å]. This suggests that the protonation of the N donor leads to more pronounced localization of the double bond at C1−C2 in **3a** than in **2a** (Scheme 8). Both NH groups interact with the BF_4^- counterions through H-bonds.

The $^{31}P\{^1H\}$ NMR spectrum of **3a** consists of a broad singlet at −34.4 ppm with ^{195}Pt satellites [^1J(P,Pt) = 1989 Hz], whereas in the ^1H NMR spectrum two triplets are assigned to the protons of the two oxazolidine CH_2 groups. The NMR data for **3a** are very similar to those of the dichloride salt reported recently,[3] except for the NMR resonance of the NH proton because of the different H-bonding interactions as a function of the counterion (see the Experimental Section). Similar spectra were observed for **3b**, although in the $^{31}P\{^1H\}$ NMR spectrum two broad, very close signals were observed (30.0 and 30.5 ppm). The two ^{31}P nuclei within each ligand are inequivalent and should give rise to an AB spin system. The singlet resonance observed for **3a** in solution may stem from accidentally identical chemical

dx.doi.org/10.1021/ic501566u | Inorg. Chem. 2014, 53, 12739−12756

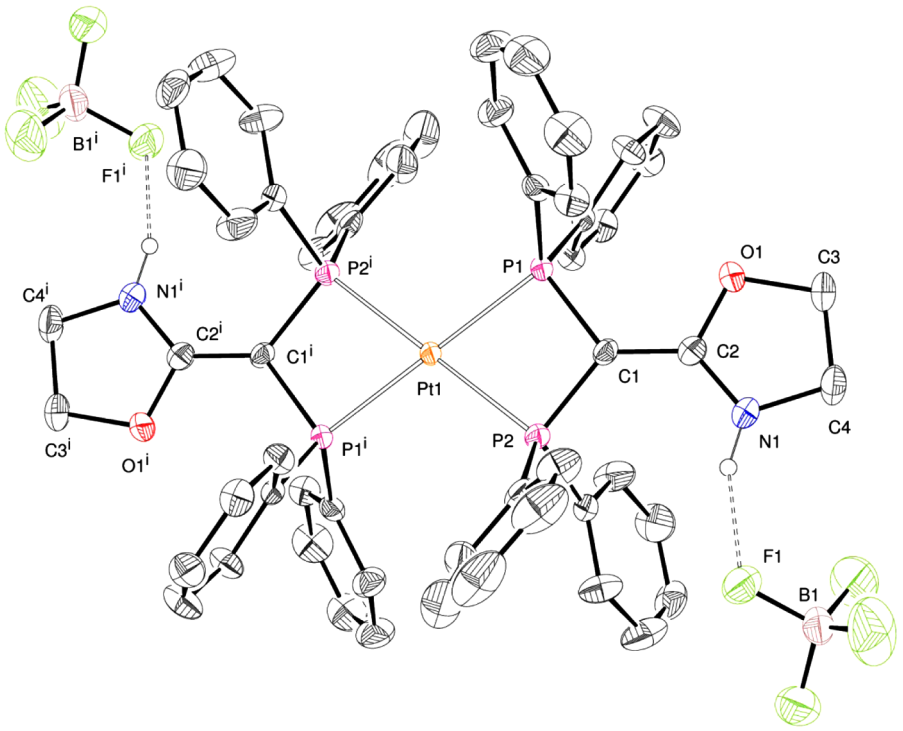

Figure 1. ORTEP of the molecular structure of **3a**. Hydrogen atoms (except those bound to N1 and N1^{i}) and solvent molecules have been omitted for clarity. Ellipsoids include 40% of the electron density. Selected distances (Å) and angles (deg): Pt1−P1 2.3267(9), Pt1−P2 2.3276(9), P1−C1 1.770(4), P2−C1 1.762(3), C1−C2 1.386(5), N1−C2 1.314(5), C2−O1 1.348(4), N1−C4 1.456(5), O1−C3 1.471(4), C3−C4 1.508(6); P2−Pt1−P1 72.01(3), C1−P1−Pt1 93.13(11), C1−P2−Pt1 93.32(12), P1−Pt1−P2^{i} 107.99(3), N1−C2−C1 130.0(3), O1−C2−C1 118.7(3), C2−C1−P1 126.4(3), C2−C1−P2 129.8(3), P1−C1−P2 101.54(17).

Scheme 10. Fast Rotation (on the ^{1}H NMR Time Scale) of the Oxazolidine Rings about the C1−C2 Bond

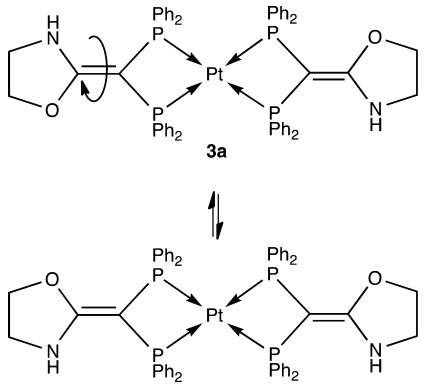

shifts for the aforementioned P nuclei or from fast rotation (on the H NMR time scale) of the oxazolidine rings about the C1−C2 bond (Scheme 10), whereas, as mentioned above, two resonances were indeed observed for **3b**. These two signals coalesce at 308(1) K [$\Delta G^{\ddagger}$ = 60(1) kJ mol^{-1}] and give rise to a sharp singlet at higher temperatures. The higher coalescence temperature of these signals for **3b** compared with the deprotonated analogue **2b**,[3] for which splitting was not observed at low temperature, is consistent with increased double-bond character of the C1−C2 bond in **3b** with respect to **2b**.

We have discussed elsewhere the influence of the substituent of the PCP carbon (e.g., oxazolidine in **3a**) in functionalized diphosphinomethanide complexes on the electronic delocalization over the P---C---C---P group.[3] Since we expected this P---C---C---P system to be the likely chromophore in the Pt(II) complex (see Photophysical Studies below), we became interested in tuning this electronic delocalization by replacing the oxazolyl group in **1** with the aromatic 4-pyridyl moiety.

Thus, the related functionalized dppm ligand 4-{bis(diphenylphosphino)methyl}pyridine (**4**) was synthesized by a two-step reaction involving (*i*) lithiation of 4-picoline using 2 equiv of *n*-BuLi and (*ii*) phosphorylation with 2.1 equiv of Ph_2PCl (Scheme 11). It is likely that the reaction involves double

Scheme 11. Synthesis of the Functionalized dppm Ligand 4-{Bis(diphenylphosphino)methyl}pyridine (4)

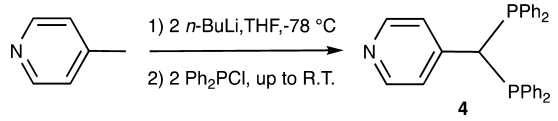

lithiation of 4-picoline, since a lithiation/phosphorylation/second lithiation/second phosphorylation pathway would likely result in the formation of diphenylphosphinobutane as a side product, which was not observed. In contrast to the rich coordination chemistry that has been developed with 2-{bis(diphenylphosphino)methyl}pyridine,[7−9,16] its isomeric ligand **4** is new, to the best of our knowledge.

In the ^{31}P{^{1}H} NMR spectrum of **4**, the phosphorus nuclei resonate at 3.3 ppm as a singlet. In the ^{1}H NMR spectrum, the four hydrogen atoms of the pyridine give rise to a complicated AA′BB′XX′ pattern due to the presence of ^{4}J(H,P) and ^{5}J(H,P) couplings.

Neutral Pt(II) and Pd(II) complexes containing the ligand bis(diphenylphosphino)(pyridin-4-yl)methanide) (**4**$_{-H}$), formed

dx.doi.org/10.1021/ic501566u | *Inorg. Chem.* 2014, 53, 12739−12756

Scheme 12. Reactions of 4 with 2 equiv of $[PtCl_2(NCPh)_2]$ (in the Presence of NEt_3) and $[Pd(acac)_2]$ (acac = Acetylacetonate) To Give 5a and 5b, Respectively

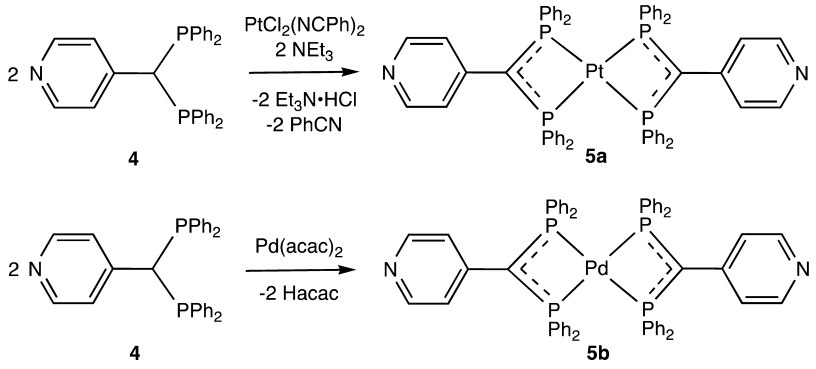

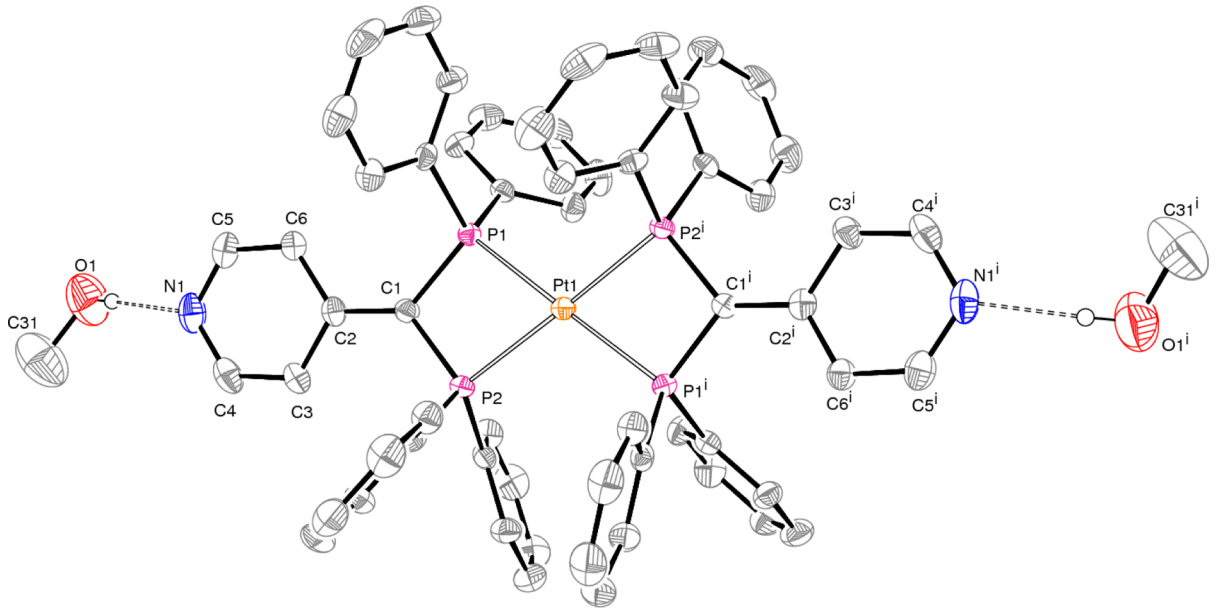

Figure 2. ORTEP of the molecular structure of **5a**·2MeOH. Hydrogen atoms (except for those involved in H-bonds) have been omitted for clarity. Ellipsoids include 40% of the electron density. Selected distances (Å) and angles (deg): Pt1−P1 2.3045(10), Pt1−P2 2.3112(11), P1−C1 1.758(4), P2−C1 1.762(4), C1−C2 1.433(6); P2−Pt1−P1 71.08(4), P2−C1−P1 99.3(2), C1−P1−Pt1 94.94(14), C1−P2−Pt1 94.61(15), C2−C1−P1 130.5(3), C2−C1−P2 130.1(3).

by deprotonation of **4**, were readily obtained. Thus, the reaction of **4** (in slight excess to facilitate purification; see the Experimental Section) with 2 equiv of $[PtCl_2(NCPh)_2]$ in the presence of NEt_3 gave $[Pt(\mathbf{4}_{-H})_2]$ (**5a**) in high yield (Scheme 12). The analogous Pd(II) complex $[Pd(\mathbf{4}_{-H})_2]$ (**5b**) was obtained quantitatively by the 2.2:1 reaction of **4** with $[Pd(acac)_2]$ (acac = acetylacetonate), in which acac acted as an internal base (Scheme 12). Complex **5a** was crystallized as **5a**·2MeOH by slow evaporation of a saturated 1:1 CH_2Cl_2/MeOH solution.

In the centrosymmetric molecular structure of complex **5a** in **5a**·2MeOH (Figure 2), two $\mathbf{4}_{-H}$ ligands bis-chelate the metal center through the phosphorus atoms, generating a distorted planar coordination environment for the metal. The P1−Pt1−P2 chelating bite angle is 71.08(4)°, and the P1−C1−P2 angle is 99.3(2)°. The pyridine ring is almost coplanar with the P1−C1−P2 group [angle between the mean planes = 9.18(4)°]. On the basis of the C1−C2 [1.433(6) Å] and P−C [P1−C1 = 1.758(4) Å and P2−C2 = 1.762(4) Å] distances, which are significantly shorter than typical C−C and C−P single bonds, respectively, it is reasonable to suggest delocalization of the double bond over the P1−C1(C2)−P2 group. This feature is similar to that encountered in a related Pt(II) phosphine complex.[7] The geometry around the C1 atom is planar [sum of the angles around C1 = 359.9(3)°]. Two molecules of methanol interact with the N atoms through H-bonds.

The $^{31}P\{^1H\}$ NMR spectrum of **5a** in solution is fully consistent with the X-ray structure shown in Figure 2. The phosphorus nuclei resonate at −33.9 ppm with ^{195}Pt satellites. The $^1J(^{31}P,^{195}Pt)$ coupling constant of 1950 Hz is typical for a *trans*-P−Pt−P arrangement.[3,17] In the ^1H NMR spectrum, there is no resonance corresponding to a methine proton, in agreement with its deprotonation. The $^{31}P\{^1H\}$ spectrum of **5b** consists of a singlet at −29.5 ppm.

In complexes **5a** and **5b**, ligand **4** is coordinated to the metal in its deprotonated form $\mathbf{4}_{-H}$. Complexes featuring the related isomeric ligand bis(diphenylphosphino)(pyridin-2-yl)methanide derived from 2-{bis(diphenylphosphino)methyl}pyridine[7−9,16] have been observed in only a few cases and resulted from a hydrogen shift from the PCP carbon to the metal center (Pt/Ir) instead of deprotonation with a base. This type of tautomerism was observed when the reaction of **1** with $[PtCl_2(NCPh)_2]$ was performed in the absence of base.[3] When **4** was added to

dx.doi.org/10.1021/ic501566u | *Inorg. Chem.* 2014, 53, 12739−12756

Scheme 13. Reactions of 4 with $[PtCl_2(NCPh)_2]$ and $[PdCl_2(NCPh)_2]$ in THF To Afford the Complexes 5a·2HCl (6a) and 5b·2HCl (6b), in Which the Proton of the PCHP Ligand Has Migrated to the Pyridine Nitrogen Atom

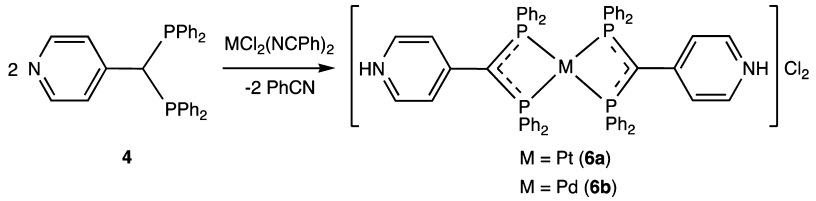

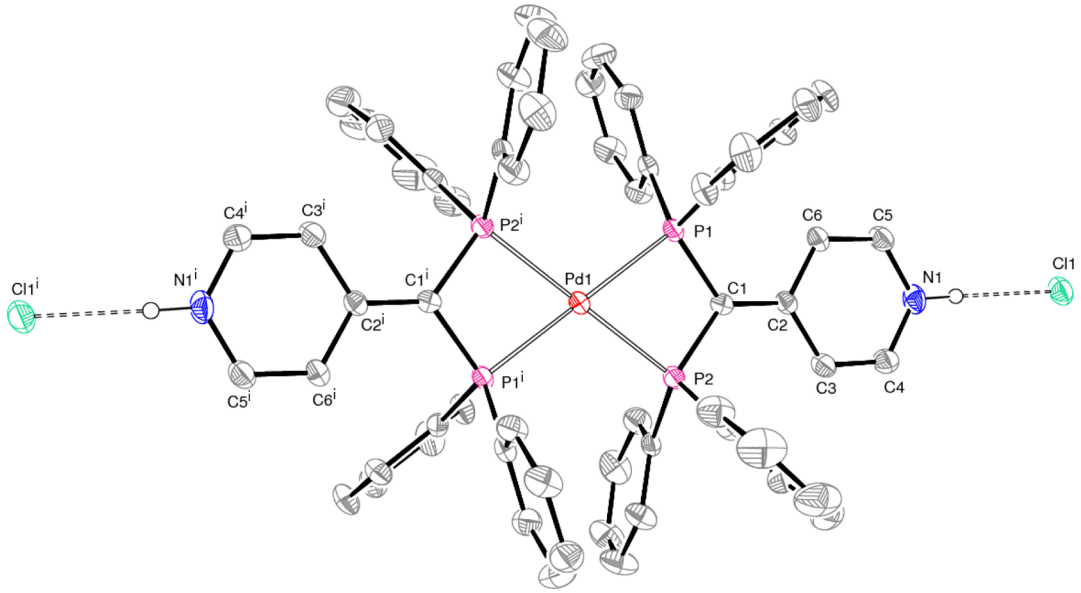

Figure 3. ORTEP of the molecular structure of **6b** in **6b**·$4CH_2Cl_2$. Hydrogen atoms (except those bound to N atoms) and solvent molecules have been omitted for clarity. Ellipsoids include 40% of the electron density. Selected distances (Å) and angles (deg): Pd1−P1 2.3093(10), Pd1−P2 2.3247(10), P1−C1 1.775(4), P2−C1 1.772(4), C1−C2 1.415(5); P2−Pd1−P1 71.38(3), P2−C1−P1 99.3(2), C1−P1−Pd1 94.03(13), C1−P2−Pd1 93.58(13), C2−C1−P1 128.5(3), C2−C1−P2 131.2(3).

$[PtCl_2(NCPh)_2]$ or $[PdCl_2(NCPh)_2]$ in tetrahydrofuran (THF), **5a**·2HCl (**6a**) and **5b**·2HCl (**6b**) were isolated as the only products (Scheme 13). Complexes **6a** and **6b** can be viewed as the dihydrochloride derivatives of **5a** and **5b**, and these complexes can indeed be easily interconverted upon deprotonation/protonation in the presence of NEt_3/HCl, respectively.

The molecular structure of **6b** was determined by X-ray diffraction methods (Figure 3). The centrosymmetric molecular structure of **6b** in **6b**·$4CH_2Cl_2$ is similar to that of **5a**, but with protonated N atoms. The structural parameters within the P1−C1(C2)−P2 moiety show only very slight changes compared with those in **5a**. The NH functions are involved in H-bonding interactions with neighboring Cl^- counterions. A C to N proton shift has occurred, from the PCP carbon to the pyridyl nitrogen. Interestingly, this tautomerism has not been observed in the case of the isomeric ligand bis(diphenylphosphino)(pyridin-2-yl)-methanide and the related ligand bis(diisopropylphosphino)-(pyridin-2-yl)methanide. For example, the complex $[Pd\{(i\text{-}Pr_2P)_2CH\text{-}2\text{-}Py\}]Br_2$[18] contains an sp^3 PCHP carbon and a nonprotonated pyridyl group both in solution and in the solid state. Compared with this latter complex, the C1−C2 bond [1.415(5) Å] and the C−P bonds of the PCP unit [P1−C1 = 1.775(4) Å, P2−C1 = 1.772(4) Å] in **6b** are significantly shorter (selected bond distances are compared in Table 2). As expected, deprotonation of the PCP carbon dramatically influences the structural properties of the P1−C1(C2)−P2 group. In $[Pd\{(i\text{-}Pr_2P)_2CH\text{-}2\text{-}Py\}]Br_2$ the C−C and C−P bonds retain their single-bond character, whereas in **6b** deprotonation of the PCP carbon leads to pronounced electronic delocalization over the P1−C1(C2)−P2 group.

Table 2. Selected Bond Distances (in Å) for 6b and the Related Pd(II)−Phosphine Complex $[Pd\{(i\text{-}Pr_2P)_2CH\text{-}2\text{-}Py\}]Br_2$, Together with a Common Atom Numbering Scheme (Substituents on P Atoms and C2 Omitted)

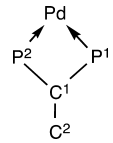

bond	**6b**	$[Pd\{(i\text{-}Pr_2P)_2CH\text{-}2\text{-}Py\}]Br_2$[a]
C1−P1	1.775(4)	1.865(4)
C1−P2	1.772(4)	1.862(4)
C1−C2	1.415(5)	1.502[b]

[a]Data from ref 18. [b]The uncertainty of this measurement was not given.

Since both **6b** and $[Pd\{(i\text{-}Pr_2P)_2CH\text{-}2\text{-}Py\}]Br_2$ contain the same metal, the C to N hydrogen transfer is probably not metal-induced because the hydrogen transfer observed in **6b** has never been observed in the case of 2-{bis(diphenylphosphino)-methyl}pyridine (i.e., with the N atom at the ortho position). The basicities of 2-picoline and 4-picoline are similar,[19] and this is likely also to be the case for the isomeric couple **4** and

dx.doi.org/10.1021/ic501566u | Inorg. Chem. 2014, 53, 12739−12756

Scheme 14. Selective Coordination of Bis(diphenylphosphino)methanephosphonate-Based Ligands $(Ph_2P)_2CHP(O)(OMe)_2$ to Pd(II) Center, Resulting in Four-Membered-Ring Chelates

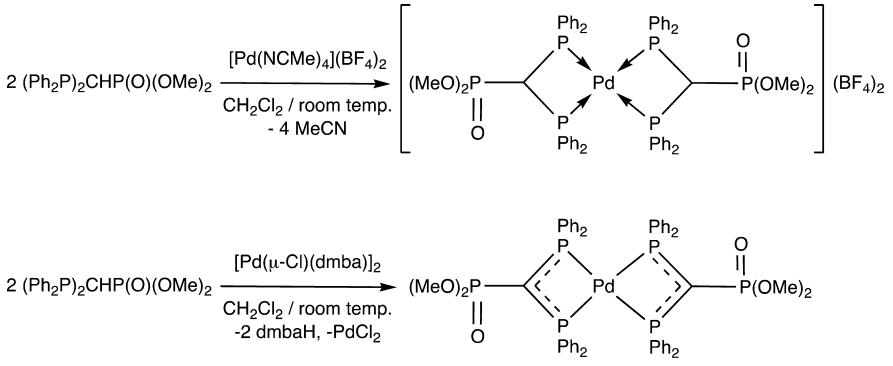

Table 3. Selected Experimental and Calculated Bond Distances (Å) of Ligands 1 and 4 and Complexes 2a, 2b, 3a, 5a, 5b, and 6a

	1	2b		2a		3a	
bond	calcd	exptl[a]	calcd	exptl[a]	calcd	exptl	calcd
M−P1		2.3219(7)	2.375	2.3164(6)	2.374	2.3267(9)	2.372
M−P2		2.3391(7)	2.386	2.3293(6)	2.379	2.3276(9)	2.369
P1−C1	1.787	1.748(3)	1.754	1.751(2)	1.752	1.770(4)	1.789
P2−C1	1.784	1.751(3)	1.759	1.745(3)	1.757	1.762(3)	1.787
C1−C2	1.430	1.432(4)	1.437	1.432(3)	1.433	1.386(5)	1.388
C2−O	1.402	1.362(4)	1.384	1.356(3)	1.385	1.348(4)	1.337
C2−N	1.293	1.291(4)	1.282	1.299(3)	1.283	1.314(5)	1.337
	4	**5a**		**5b**		**6a**	
bond	calcd	exptl	calcd	exptl	calcd	exptl	calcd
M−P1		2.305	2.369	–	2.370	–	2.359
M−P2		2.311	2.375	–	2.369	–	2.370
P1−C1	–	1.758	1.755	–	1.761	–	1.794
P2−C1	–	1.762	1.757	–	1.767	–	1.795
C1−C2	–	1.433	1.453	–	1.451	–	1.403

[a]Data from ref 3.

2-{bis(diphenylphosphino)methyl}pyridine. A recent work showed that the tautomerization of both 2- and 4-hydroxypyridine to the corresponding pyridones was similarly energetically favored.[20] The C to N hydrogen shift observed in **6b** may thus be favored by the additional stabilization provided by nonclassical H-bonds (see Figure 3), which would not be available in the case of 2-{bis(diphenylphosphino)methyl}pyridine because of the steric hindrance exerted by the P substituents. Recently, related tautomerizations involving N to N hydrogen migration were observed in 2-aminooxazoline−[21] and 2-aminothiazoline−metal-containing systems.[22]

In solution, the two cationic complexes **6a** and **6b** show NMR spectra fully consistent with their solid-state structures. In the $^{31}P\{^1H\}$ spectrum of **6a**, the phosphorus atoms resonate at −31.4 ppm, and the corresponding $^1J(^{31}P,^{195}Pt)$ coupling constant of 1975 Hz is consistent with the trans influence exerted by the P atoms. The $^{31}P\{^1H\}$ spectrum of **6b** consists of a singlet at −28.5 ppm. The pattern of the ^1H NMR resonance for the H3 and H6 protons is shielded and overlaps with the signals of the phenyls in comparison with those of **5a** and **5b**, suggesting a pronounced electronic effect exerted by the protonation of the N atoms.

Interestingly, in previous studies of related functional shortbite ligands it was found that bis(diphenylphosphino)-methanephosphonate-based ligands $(Ph_2P)_2CHP(O)(OMe)_2$ form metal complexes by selective coordination of the diphosphine moiety to Pd(II) and Ni(II) centers, resulting in four-membered-ring chelates (Scheme 14).[23] Spontaneous deprotonation of these ligands at the PCHP site occurred when a basic ligand was present in the precursor metal complex, such as 2-{(dimethylamino)methyl}phenyl-κ^2-C^1,N (dmba) or methyl in the case of Pd(II) or acac in the case of Ni(II).

B. Experimetal and Theoretical Studies of the Optical Properties. The absorption and emission spectroscopy of **2a** and **2b** (Scheme 5) and of **5a** and **5b** (Scheme 12) were analyzed by means of a combined experimental and theoretical investigation.

Structural Properties of the Electronic Ground States. The optimized structural parameters of main interest for the PCP-oxazoline (**2a** and **2b**)- and PCP-pyridine (**5a** and **5b**)-substituted complexes are reported in Table 3, along with the X-ray data for comparison. The atom numbering is defined according to the models depicted in Figure 4. The theoretical values agree rather well with the experimental data, validating the computational strategy. However, the theoretical bond lengths obtained in vacuum are slightly overestimated with respect to the data in the solid state, as could be expected.

Surprisingly, the geometrical parameters are almost identical for the Pd(II) and Pt(II) complexes, both experimentally and theoretically. The most remarkable feature is that all of the bond lengths deviate from their usual standard values. The nature of the C_1-C_2 bond deserves some comments. In the neutral compounds, the character of this bond is intermediate between single and double (~1.43 Å). Its double-bond character increases

dx.doi.org/10.1021/ic501566u | Inorg. Chem. 2014, 53, 12739−12756

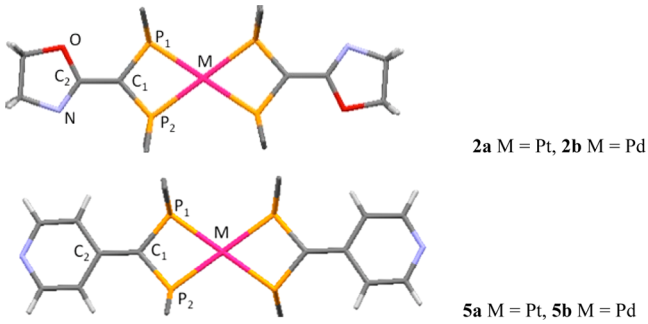

Figure 4. Schematic structures of (top) the PCP-oxazoline complexes **2a** and **2b** and (bottom) the PCP-pyridine complexes **5a** and **5b** (phenyl groups omitted for clarity).

in the protonated species (~1.39 Å). The P−C bonds are also much shorter than usual for a single bond (1.85 Å for a standard P−C bond), with some double-bond character that is weakened upon protonation. In contrast, in the neutral species (**2a**, **2b**, **5a**, and **5b**), the C−O and C−N bond lengths are almost at their standard values. Upon protonation, however, a significant shortening of the C−O bond is observed, as well as an elongation of the C−N bond. This suggests that the contribution of the nitrogen to the electronic delocalization is diminished, while that of the oxygen is increased.

All of these results suggest that in the neutral species the formal lone pair held by the carbanion is conjugated with the two phosphorus atoms and much less with the oxazoline. Upon protonation this scheme is reversed, as the oxazoline becomes more electrophilic because of its positive charges. Similar observations can be made for the PCP-pyridine derivatives.

Electronic Absorption Spectroscopy. The experimental absorption spectra of **2a**−**b**, **3a**, and **5a**−**b** in *N*,*N*-dimethylformamide (DMF), CH_2Cl_2, and toluene are shown in Figures 5 and 6, and the energies of the most prominent absorption bands and their extinction coefficients are listed in Table 4. The electronic absorption spectra of the five complexes are dominated by intense spin-allowed absorptions in the region below 350 nm, with molar extinction coefficients in the range (3.0−5.0) × 10^4 cm^{-1} M^{-1}. These bands can be assigned to spin-allowed singlet-manifold ligand-centered (^{1}LC) transitions located on the phenyls, pyridines, and linked methyldiphosphine moieties, as typical for complexes bearing aromatic rings.

Table 4. Electronic Absorption Characteristics of Complexes 2a, 2b, 3a, 5a, and 5b at Room Temperature in Different Solvents

	λ_{abs}/nm (ε/10^4 M^{-1} cm^{-1})			
complex	DMF[a]	toluene[a]	CH_2Cl_2	DMF + TFA
2a	380 (0.82), 276 (4.06)	376[br]	383	333 (0.47)
2b	428 (0.23), 365[sh] (0.85), 318 (4.79)	–	–	–
3a	385 (0.66), 276 (3.58)	–	–	–
5a	422 (1.95), 308[sh] (2.70), 285 (4.63)	429	420	414 (0.76)
5b	475[sh] (0.12), 395 (1.44), 328 (3.08)	–	–	–

[a]sh denotes a shoulder; br denotes a broad band.

All of the complexes display absorption bands in the region between 350 and 500 nm. The PCP-pyridine-substituted complexes **5a** and **5b** show intense bands in this region. In particular, compound **5a** displays an absorption band at 422 nm (ε = 1.95 × 10^4 cm^{-1} M^{-1}), while **5b** shows two bands, a higher-energy and more intense band at 395 nm (ε = 1.44 × 10^4 cm^{-1} M^{-1}) and a much weaker band at 475 nm ($\varepsilon \approx 1.2 \times 10^3$ cm^{-1} M^{-1}).

The absorption spectra of the PCP-oxazoline-substituted complexes **2a** and **2b** show slightly different behavior around 400 nm (Figure 5). The spectrum of **2a** shows one definable absorption band at 380 nm ($\varepsilon \approx 8 \times 10^3$ cm^{-1} M^{-1}) with a tail that extends to around 450 nm. The similarity of the absorption spectra of **3a** and **2a**, which display almost identical absorption features and absorption coefficients, suggests that **3a** exists as the nonprotonated form in dilute solution. The absorption spectrum of **2b** is characterized by two distinct absorption bands, a higher-energy shoulder at around 365 nm (ε = 8.5 × 10^3 cm^{-1} M^{-1}) and a lower-energy band at 428 nm (ε = 2.8 × 10^3 cm^{-1} M^{-1}), again with a tail that extends beyond 500 nm.

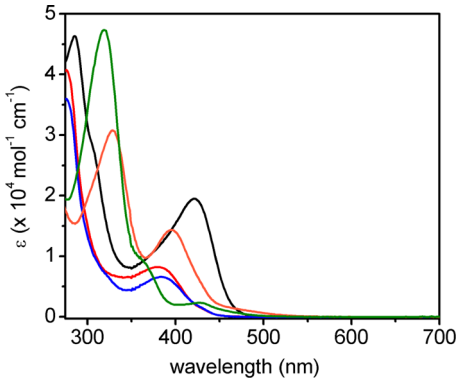

Figure 5. Absorption spectra in dilute DMF at room temperature for complexes **2a** (red trace), **2b** (green trace), **3a** (blue trace), **5a** (black trace), and **5b** (orange trace).

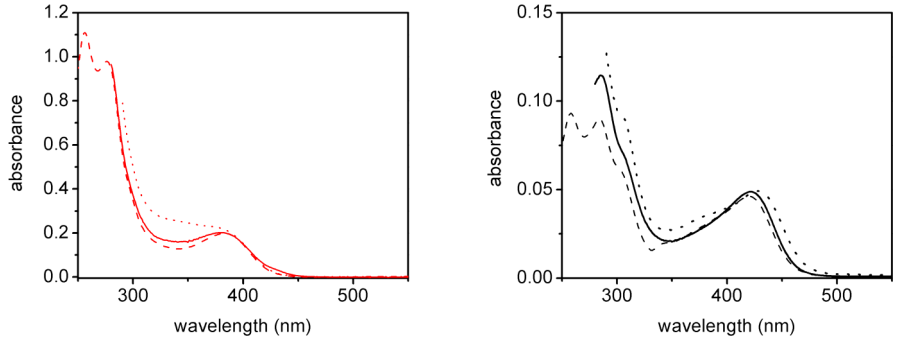

Figure 6. Absorption spectra of (left) **2a** and (right) **5a** in DMF (solid trace), CH_2Cl_2 (dashed trace), and toluene (dotted trace) at concentrations of 2.5 × 10^{-5} and 2.5 × 10^{-6} M for **2a** and **5a**, respectively.

dx.doi.org/10.1021/ic501566u | *Inorg. Chem.* 2014, 53, 12739−12756

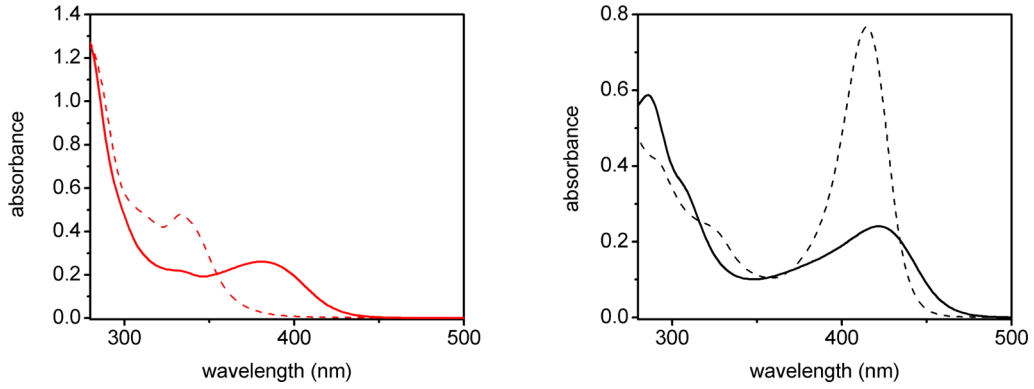

Figure 7. Absorption spectra of (left) **2a** and (right) **5a** in dilute DMF solution before (solid trace) and after (dashed trace) addition of an excess of TFA (1000 equiv).

Comparison with the deprotonated free ligand[24] proves that these more intense bands in the region above 350 nm in the Pt−PCP-pyridine and Pd−PCP-pyridine complexes possess significant ^{1}LC character perturbed by the metal (data not shown).

Complexes **5a** and **5b** are characterized by absorption bands lying at lower energy than for the ligand, which displays one band at 378 nm. The energy differences (peak to peak) between the lowest-energy ligand absorption band and the lowest-energy intense absorption for the two complexes are about 2700 and 1100 cm^{-1} for **5a** and **5b**, respectively. This trend is in accordance with observations made for related palladium and platinum complexes, where metal-to-ligand charge transfer (MLCT) bands occur at higher energy in the former than in the latter as a result of the higher oxidation potentials of Pd(II) versus Pt(II).[25] Like the oxazoline-containing complexes **2a** and **2b**, both pyridine derivatives **5a** and **5b** exhibit absorption tails extending toward the red that do not show clearly distinguishable bands.

Also, the possibility of having low-energy MLCT transitions localized on the oxazoline moieties can be excluded. Even though the addition of an excess of protons in the form of trifluoroacetic acid (TFA) (1000 equiv) could lead to degradation, the analysis of the spectral modifications may help in the assignment. Indeed, upon addition of TFA to dilute DMF solutions of the PCP-oxazoline substituted complexes **2a** and **2b**, depletion of these lower-energy absorption bands is clearly observed, yielding a hypsochromically shifted absorption maximum centered at 333 nm for **3a** (Figure 7 left). After removal of these intense visible transitions, there is still observable absorbance in the region between 333 and 425 nm, probably due to residual unprotonated species. Indeed, the theoretical spectrum (vide infra) of **3a**, the protonated form of complex **2a**, does not indicate the presence of metal-centered (MC) states in this region, while an excitation process lying at 329 nm was computed, in good agreement with the experimental value (333 nm).

Protons are indeed expected to coordinate the free nitrogen atoms on the pyridines in complexes **5a** and **5b** much better than the oxazoline moieties of complexes **2a** and **2b**. The change in electron density associated with this coordination should allow us to determine the contributions of the pyridine and the oxazoline to excitation originating from the π-delocalized system. The change in the absorption spectrum upon addition of protons in the form of TFA to a DMF solution of complex **2a** is very dramatic, showing the disappearance of the band at 380 nm and the formation of the absorption at 330 nm (Figure 7). The observed changes can be attributed to the modification in the electron-donating ability of the oxazoline, which upon protonation cannot act as a donor, reducing the σ donation of the coordinated phosphine. Therefore, the band in the visible region for the nonprotonated species must possess strong ligand-to-metal charge transfer (LMCT) character. In a similar way, upon protonation of the pyridine ring, the formation of a double bond between C1 and C2 (Table 2) leads to a more localized but higher-energy transition with an oscillator strength, shown as a sizable increase of the intensity of the lowest-energy absorption band observed at 422 nm. For complex **5a**, the small hypsochromic shift (340 cm^{-1}) is due to the very weak basicity and electron-donating nature of the five-membered ring. This blue shift is qualitatively reproduced by time-dependent density functional theory (TD-DFT) calculations (vide infra), even though it is significantly overestimated (~3000 cm^{-1}). Accordingly, the contribution of the pyridilic ring to the lowest-energy transition in PCP-pyridine complexes is less significant than that of oxazoline moiety in the corresponding complexes **2a** and **2b**.

The theoretical absorption spectra of the neutral complexes (**2a**/**2b** and **5a**/**5b**) and those of the protonated platinum derivatives (**3a** and **6a**) calculated using TD-DFT in DMF are depicted in Figure 8 (for **2a**, **2b**, and **3a**) and Figure 9 (for **5a**, **5b**, and **6a**). The spectra were computed on the optimized structures of the electronic ground states reported in Table 3. The complete

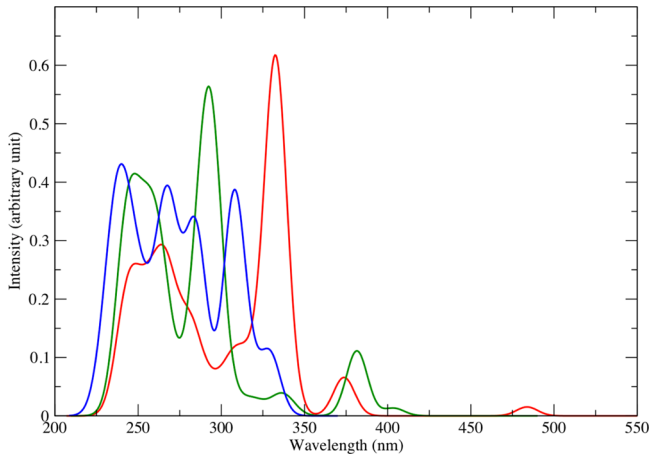

Figure 8. Theoretical absorption spectra of PCP-oxazoline complexes **2a** (blue trace), **2b** (red trace), and **3a** (green trace), including solvent corrections (DMF).

dx.doi.org/10.1021/ic501566u | *Inorg. Chem.* 2014, 53, 12739−12756

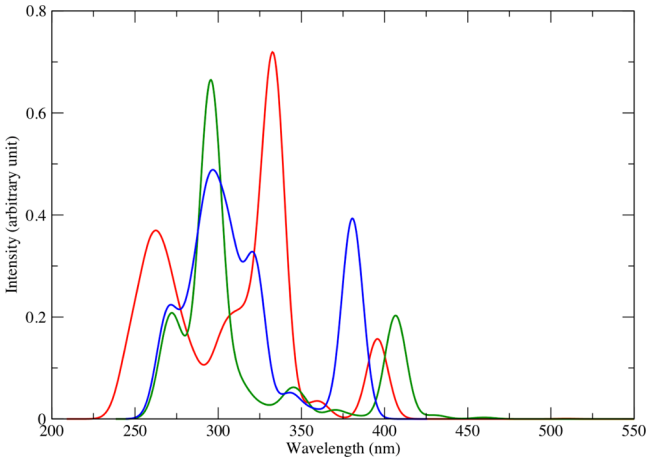

Figure 9. Theoretical absorption spectra of the PCP-pyridine complexes **5a** (blue trace), **5b** (red trace), and **6a** (green trace), including solvent corrections (DMF).

theoretical data, including oscillator strengths and electron density differences that characterize the electronic transitions, are reported in the Supporting Information. In line with the experimental results, the spectra of the oxazoline-containing complexes show similar features, with a red shift of the lowest weak absorption band of the palladium complex (484 nm) with respect to the platinum counterpart (404 nm).

The calculated transition energies listed in Table 5 are compared to the observed absorption maxima and show rather good agreement between the theoretical and experimental absorption spectra as far as the intense bands are concerned (Table 5). The lowest-energy theoretical transitions are very weak; they were not observed in the Pt complexes (**5a** and **2a**) and are bathochromically shifted compared with the experimental maxima observed in the Pd complexes (**5b** and **2b**).

Table 5. Comparison between Experimental and Theoretical Absorption Transitions (λ_{abs}, in nm) of the PCP-Oxazoline Complexes (2a, 2b, and 3a) and PCP-Pyridine Derivatives (5a, 5b, and 6a) in DMF as the Solvent (The Complete Data, Including Oscillator Strengths and Differences in Electron Densities Characterizing the Electronic Transitions, Are Reported in the Supporting Information)

2b		**2a**		**3a**	
exptl	calcd	exptl	calcd	exptl	calcd
475	469		396	333	332
428	–				
365	366	380	376		319
318	328	276	294		305
5b		**5a**		**6a**	
exptl	calcd	exptl	calcd	exptl	calcd
475	468		395	414	381
395	376	422	429		319
328	335	308	289		
		285			

For the sake of clarity, only the transitions for the PCP-oxazoline complexes **2a** and **2b** are listed. The other neutral complexes show the same optical trends. The two first theoretical transitions of **2a** and **2b** are similar in character. This character is illustrated by the electron density differences depicted in Figure 10 for the two lowest-energy transitions of **2b** calculated at 469 and 366 nm. As suggested by experimental evidence, these transitions have LC character with a significant LMCT contribution. The leaving electron comes from the same π_L orbital purely localized on the ligand, with the largest contribution coming from the anionic carbon and the oxazoline nitrogen. The weak absorptions from S_1 (LMCTσ) states calculated at 469 (f = 0.015) (**2b**) and 396 nm (f = 0.011) (**2a**) correspond to excitations from the carbanion to a mixed M−P antibonding orbital delocalized over the metal and the P atoms. The next most intense transitions from S_2 (LMCTπ) states calculated at 366 nm (f = 0.071) (**2b**) and 376 nm (f = 0.119) (**2a**) correspond to excitations to π bonding orbitals between the phosphorus atoms and the pπ orbitals of the metal atoms accompanied by delocalization over the P-bound phenyls.

Analysis of the theoretical results obtained for the pyridine-substituted complexes **5a** and **5b** leads to similar absorption properties. These results support the experimental analysis of the absorption spectra of complexes **5a** and **5b** with respect to the absorption spectrum of the free ligand. Indeed, the absorption of the free ligand corresponds to an excitation from the anionic carbon and the nitrogen atom toward the phenyl groups. Upon complexation, the two lowest-energy bands in the complexes still present partially this character with no metal bonding or antibonding contribution.

The highest-energy experimental peaks, observed below 330 nm, can be assigned to a combination of three transitions of mixed LC and LMCT character. These processes correspond to an excitation from the π system of the conjugated anionic carbon and the oxazoline to a delocalized orbital over the metal center and the ligands. The picture is similar for all of the complexes, though the LC character in the PCP-pyridine complexes is enhanced.

The lowest-energy bands are bathochromically shifted in the PCP-pyridine complexes compared with the PCP-oxazoline counterparts, in agreement with the experimental findings (see Table 5). This could be explained by the low contribution of the pyridine in the donating orbital in the two lowest-energy LMCT transitions.

Complex **6a** is the only exception to this general scheme, since the metal contribution to the lowest-energy virtual orbitals decreases significantly upon protonation. Consequently, the absorption bands of the protonated species **6a** become nearly pure IL in nature. The details of the theoretical results are reported in the Supporting Information.

Luminescence Properties. All of the investigated complexes, namely, **2a**, **2b**, **3a**, **5a**, and **5b**, are emissive at 77 K in a DMF glassy matrix, in the pure solid state, and when used as dopants into poly(methyl methacrylate) (PMMA) thin films, but they do not show any detectable emission in fluid solution at room temperature. Such a lack of luminescence in solution suggests the following possibilities: (*i*) solvent interactions efficiently quench the excited state; (*ii*) the relatively flexible nature of the ligands quenches the emission; and (*iii*) the emissive states are highly distorted. All of these radiationless deactivation pathways should be significantly reduced in the solid state and at 77 K in a glassy matrix, restoring the emission properties of the complexes.

In square-planar complexes, solvent quenching is expected to occur through interactions at the exposed axial positions of the complexes. However, it would be surprising that in these complexes this mechanism would be so efficient, considering that the axial positions seem to be efficiently screened by the phosphine phenyls (see the crystal structures), suggesting that

dx.doi.org/10.1021/ic501566u | *Inorg. Chem.* 2014, 53, 12739−12756

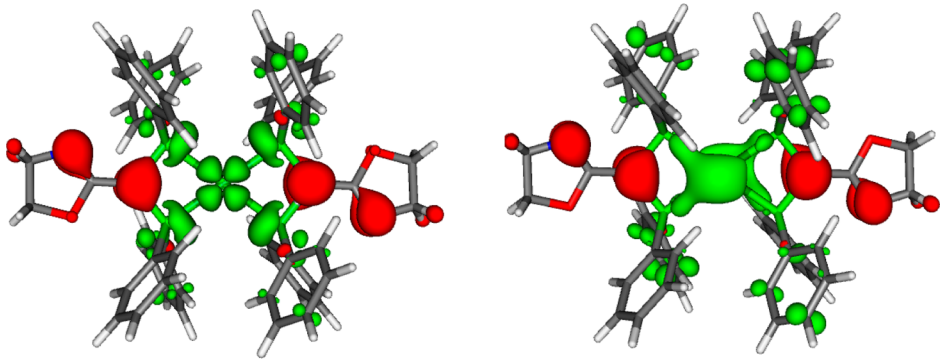

Figure 10. Plots of the differences in electron density characterizing the electronic transitions at (left) 469 and (right) 366 nm for complex **2b**. Areas of increasing and decreasing density are displayed in green and red, respectively.

Table 6. Photophysical Data for Complexes 2a, 2b, 3a, 5a, and 5b in DMF Frozen Solution at 77 K, in the Solid State, and in PMMA at a Doping Level of 5 wt %

	77 K		solid state			5 wt % in PMMA		
complex	λ_{em} (nm)	τ (μs)	λ_{em} (nm)	τ (μs)	PLQY (%)	λ_{em} (nm)	τ (μs)	PLQY (%)
2a	572	91.7	537	3.6 (27%)	29	536	6.2 (14%)	21
				13.1 (73%)			20.0 (86%)	
2b	660	79.3 (62%)	654	2.8 (29%)	5	657	0.1 (19%)	1
		30.9 (38%)		7.4 (71%)			0.45 (81%)	
3a	572	90.8	515	1.1 (27%)	1	–[a]	–[a]	–[a]
				12.0 (72%)				
5a	569	97.8	610	2.0 (31%)	18	559	5.6 (23%)	40
				7.0 (69%)			15.5 (77%)	
5b	675	168 (31%)	607	0.62 (34%)	10	647	0.55 (42%)	7
		513 (69%)		1.4 (66%)			1.6 (58%)	

[a]The sample did not show any detectable emission.

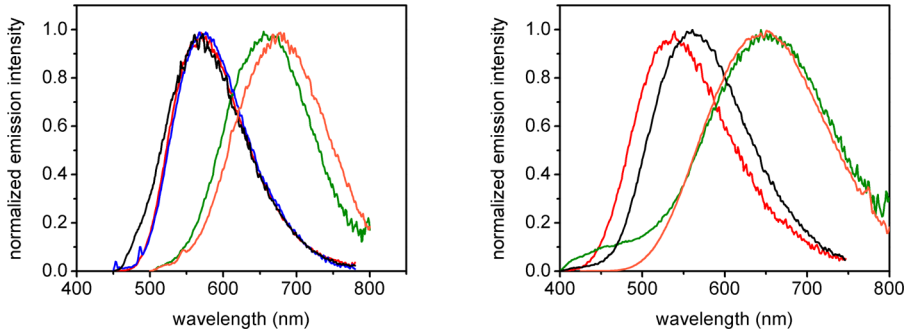

Figure 11. Emission spectra in (left) DMF glassy matrixes at 77 K and (right) PMMA thin films at 5 wt % doping level for complexes **2a** (red trace), **2b** (green trace), **3a** (blue trace), **5a** (black trace), and **5b** (orange trace). The 77 K and thin-film samples were excited at λ_{exc} = 425 and 375 nm, respectively.

the distortion of the complex upon excitation is important. This is supported by the nature of the first emitting states that arise from the absorbing transitions, the first one being σ_{M-P} antibonding in nature and the second one having π bonding character.

The steady-state emission data for the complexes at 77 K in DMF, in the pristine solid state, and in PMMA thin films are given in Table 6, and the emission spectra are shown in Figure 11. The corresponding emission spectra of the pristine solid-state samples are reported in Figure S1 in the Supporting Information. As far as emission in the DMF glassy matrix at 77 K is concerned, all of the investigated complexes display intense, broad, and structureless emission profiles centered in the region 569–675 nm.

Complexes **2a** and **3a** show identical emission spectra in DMF at 77 K, with emission maxima centered at 572 nm, due to the unprotonated nature of **3a** in dilute DMF solution. This finding is similar to the one observed in the absorption spectra for the same complexes. The spectrum of the Pd(II) analogue, complex **2b,** displays a bathochromically shifted emission with respect to **2a** with a maximum centered at 660 nm. The PCP-pyridine-substituted complexes **5a** and **5b** display emission profiles very similar to those of their oxazoline counterparts, with emission maxima at 569 and 675 nm, respectively. This bathochromic shift is reproduced by the calculations for both the S_1 state and the lowest emissive T_1 state (vide infra).

For the PCP-pyridine complexes, the emission spectra are mostly ^{3}LMCT and not ligand-centered in character, as the

dx.doi.org/10.1021/ic501566u | *Inorg. Chem.* 2014, 53, 12739–12756

emission wavelengths for both the Pt(II) and Pd(II) complexes are strongly bathochromically shifted by 3350 and 6100 cm^{-1} for **5a** and **5b**, respectively, with respect to the emission of the free deprotonated ligand (present work, 478 nm; also see ref 23). Indeed, the theoretical analysis indicates that the lowest states contributing to the emission band have LMCT character with an electronic distribution very similar to that of the lowest-energy S_1 and T_1 transitions.

Three interesting features can be extracted from the emission properties: (*i*) replacement of the oxazoline by a pyridine ring on the methyldiphosphine group has little effect on the steady-state luminescence features; (*ii*) the emission spectra are broad and structureless; and (*iii*) the influence of the metal center on the emission characteristics is significant, with a sizable bathochromic shift observed in going from Pt to Pd.

The first point suggests that the excited state does not extend onto the substituents of the methyldiphosphine moieties. However, it is clear from the crystal structure that for both substituent types, efficient overlap of the oxazoline or pyridine with the conjugated methyldiphosphine group can be envisaged, since the two-ring systems are coplanar with respect to the metal coordination plane, leading to strong electronic communication between these moieties. This effect is observed in the intense high-energy bands of the absorption spectrum, where bands of the PCP-pyridine complexes are bathochromically shifted with respect to the absorption bands of the PCP-oxazoline complexes by 27 nm (1600 cm^{-1}).

The second point is that the character of the emissive state should explain the fact that the emission spectra are broad and featureless. Other Pt and Pd complexes for which the emission recorded at 77 K has been assigned to either admixed MLCT/IL or metal-perturbed IL states display structured emission.[26−28] However, this is not the case for complexes that exhibit emission from highly distorted MC states.[27] At these temperatures, broad and featureless emission is almost always observed. For the complexes presented here, the emission bandwidths (full width at half-maximum (fwhm)) are 3750 cm^{-1} (**5a**), 3150 cm^{-1} (**5b**), 3500 cm^{-1} (**2a**), and 3200 cm^{-1} (**2b**). These values are rather similar to the bandwidths of other Pt and Pd complexes with emission assigned to MC states found in the literature.[29] However, according to the present theoretical analysis, the emissive states correspond to LMCT states with significant LC contributions.

The third point, namely the bathochromic shift of the emission of the Pd complexes with respect to the Pt complexes, is very unusual for emissive ^{3}MLCT states. The higher oxidation potential of Pd(II) with respect to Pt(II) usually results in higher-energy ^{3}MLCT emissions for Pd complexes compared with Pt complexes with the bearing ligands.[30−32] However, such modulation of the emission maxima strongly supports the idea of a significant metal contribution to the emitting excited state.

Another gauge that has been put forward to identify emission arising from a state with either MC or LMCT character is the degree of the observed Stokes shift.[33] Complexes that emit from highly distorted states, such as complexes displaying MC-based emission, are expected to show larger Stokes shifts than those emitting from (less distorted) ^{3}MLCT states. For all of the complexes, the excitation spectrum in DMF at 77 K roughly follows the corresponding absorption profile, reproducing quite well the weak tails that extend toward the lower-energy portion of the spectrum.

Typically, ^{3}MC states display very slow radiative deactivation processes under frozen conditions at 77 K,[25] while they either do not exhibit emission or emit with very fast decay kinetics at room temperature in fluid solution. With the present complexes, the emission lifetimes span from 79 to over 500 μs at 77 K in the DMF glassy matrix. In complexes where either ^{3}LMCT or ^{3}LC emissions are expected to be operative, these long excited-state lifetimes would suggest a high degree of ^{3}LC character and concomitant small contribution from the metal ion. On the basis of the above-mentioned discussion, for these complexes we have ruled out emission arising from states that are purely ^{3}LC in character on the basis of their emission band shapes, their large shifts with respect to the emission spectrum of the free ligand **4** in its deprotonated form, and the negligible sensitivity shown by the maximum of emission upon substitution at the P−C−P carbon.

In frozen DMF at 77 K, rather long excited-state lifetimes were observed for all of the investigated complexes. In particular, the Pd derivatives show biexponential decay with τ_1 = 30.9 μs (38%) and τ_2 = 79 μs (62%) for **2b** and τ_1 = 513 μs (69%) and τ_2 = 168 μs (31%), and **5b**, respectively. Furthermore, both of the corresponding platinum counterparts display monoexponential kinetics as slow as 91.7 and 97.8 μs for **2a** and **5a**, respectively.

Upon photoexcitation at 300−400 nm, solid-state samples of all the complexes display broad emission profiles with bandwidths similar to those found in frozen DMF solution (Figure S1 in the Supporting Information). It is interesting to note that there are significant changes in emission energy in going from frozen solution to the pure solid state, even though a correlation between the structural and packing parameters and the difference in emission features is still elusive. In general, in going from frozen solution to the solid state, all of the compounds except **5a** exhibit hypsochromically shifted emission maxima to different extents. It should be kept in mind that the environment in the (micro)crystalline packing as well as the amount of amorphous phase may not be the same for all of the complexes and that the emission properties might be highly sensitive to any subtle changes in such packing motifs.[34−38] For all of the complexes in the solid state, the observed emission lifetimes are biexponential and the PCP-oxazoline substituted complexes show slower kinetics than their PCP-pyridine analogues. The excited-state lifetimes are considerably shorter with respect to the low-temperature measurements but still rather long. The trend observed for the photoluminescence quantum yields (PLQYs) in the solid state does not parallel the recorded lifetimes, and complex **5a** shows the highest PLQY of 29%, while the most emissive Pd complex has an emission PLQY of 10%.

In spin-coated PMMA thin films at a doping concentration of 5 wt %, a trend in the emission energies among the different complexes can be observed, with sizable hypsochromic shifts with respect to the spectra recorded in frozen solvent. Under such conditions, complex **5a** shows a PLQY with a value as high as 40%, which is the highest among the investigated complexes, while the most emissive Pd complex **5b** displays rather similar PLQYs as a neat solid or at 5 wt % in PMMA, with values of 10% and 7%, respectively. All of the thin-film samples show excited-state lifetimes with biexponential decays.

The theoretical results support the assignments based on the experimental findings. Indeed, the LC/LMCT character of the emitting state originates from the lowest absorbing states, in agreement with the observed features described above. The theoretical emission wavelengths of complexes **2a**, **2b**, **5a**, and **5b** were computed on the basis of the optimized structures of the low-lying triplet excited states. The singlet states were extrapolated from the triplet geometries because of severe

dx.doi.org/10.1021/ic501566u | *Inorg. Chem.* 2014, 53, 12739−12756

convergence problems in the optimization procedure. Consequently, the emission energies may be overestimated for the singlet states. Table 7 reports the geometrical deformations of **2b** in going from the electronic ground state to the low-lying T_1 and T_2 excited states.

Table 7. Selected Computed Bond Distances (in Å) of 2b in the Electronic Ground State and the T_1 and T_2 Excited States (Atom Numbering Is Defined in Figure 4)

	ground state	T_1	T_2
Pd−P_1	2.375	2.485	2.352
Pd−P_2	2.386	2.462	2.355
P_1−C_1	1.754	1.795	1.791
P_2−C_1	1.759	1.796	1.786
C_1−C_2	1.437	1.420	1.417
C_2−O	1.384	1.379	1.378
C_2−N	1.282	1.317	1.318

The geometrical distortions are in line with the characteristics of the electronic transitions. For T_1 we observed a significant lengthening of the M−P bonds, consistent with population of the M−P antibonding-type orbital. Simultaneously, the C−P bonds become longer and so does the C−N bond, whereas the C−C bond is shortened. On the contrary, the deformation associated with T_2 leads to a shortening of the M−P bonds, in line with the population of a bonding π-like M−P orbital. The deformation of the ligand in the T_2 state is similar to the one in the T_1 transition. Similar modifications are observed for the computed excited-state geometries of all other species except protonated pyridine (Tables S1−S6 in the Supporting Information).

The emission wavelengths obtained both theoretically and experimentally for the different complexes are listed in Table 8

Table 8. Comparison between the Experimental and Theoretical Emission Wavelengths (in nm) of the Lowest S_1, T_1, and T_2 Excited States for 2a, 2b, 5a, and 5b (Theoretical Values Were Computed in DMF Solvent)

complex	exptl DMF 77 K	S_1 LMCTσ	T_1 LMCTσ	T_2 LMCTπ
2b	660	682	703	453
2a	572	512	520	478
5b	675	671	683	470
5a	569	547	594	

for comparison. The lowest-energy theoretical state emits at a wavelength consistent with the experimental results for the main part of the emission. Furthermore, its nature is in very good agreement with the LMCT/LC experimental assignment. According to the theoretical results, the T_1 and S_1 states corresponding to the LC/LMCTσ transitions, the electron densities of which are depicted in Figure 10 (left) for **2b** (M = Pd), mainly contribute to the emission bands. Indeed, the broad main emission peak for **2b** (green trace in Figure 11 right) presents a shoulder between 400 and 500 nm. This satellite peak seems to be roughly centered at 450 nm. According to the theoretical results, this peak could correspond to a weak emission from the second triplet state (T_2). The absence of satellite peaks for other complexes can be easily explained. In the platinum complexes (**2a** and **5a**), the separation between the two triplet states is much smaller than in **2b**, and the signal coming from T_2 could be covered by the intense T_1 band. The case of **5b** is trickier, and the most likely explanation is that its intensity is very weak.

The results presented above indicate that the absorption spectra of the neutral complexes are very similar whatever the cation or the ligand considered. The two first transitions are generated by the promotion of an electron originating from the carbanion lone pair, which is conjugated with the ligand π system. The relatively weak influence of a change in the ligand unsaturated cycle is due to their similar properties. The red-shift effect of the pyridine derivative compared with the oxazoline one for the same cation could be attributed to the greater LC character of the transition. The larger π system is able to stabilize the created positive charge.

The emission properties are governed by the first transitions S_1 and T_1, which contribute mainly to the intense experimental band. In line with the antibonding character of the orbitals, the geometries in the excited states in all cases present a strong elongation of the M−P bonds. This also explains the large experimental Stokes shift, as the structure is significantly distorted upon excitation. The weak effect of the ligand ring on the emission is easily explained by its small contribution.

The low-energy emission of the Pd(II) complexes compared with the Pt(II) complexes is easily explained in terms of bonding interactions. Indeed, the two complexes have the same formal $(n-1)d^8\ ns^0\ np^0$ electron configuration, with $n = 5$ for Pd and $n = 6$ for Pt, but the formally empty 6s Pt orbital is more electrophilic than the Pd 5s orbital. This favors charge transfer toward the metal for the Pt complexes. This electronic structure explains the similarity of the bond lengths despite the increasing size of the cation: the greater charge transfer contribution counterbalances the greater Pauli repulsion between the occupied shells of the fragment. Also, the Pt 5d orbitals are more diffuse than the Pd 4d orbitals.[39] The similarity of the bond lengths means that the last empty metal d orbital is much more destabilized for M = Pt than for M = Pd. Consequently, its population is energetically more costly for M = Pt than for M = Pd. This is the origin of the absorption blue shift for the Pt complexes compared with the Pd complexes.

This analysis may also explain the emissive properties of the Pt complexes. Indeed, upon relaxation, the bond length elongation due to population of the d orbitals weakens the charge transfer between the anionic ligand and the cation, which is strongly dependent on the interatomic distance. In the Pt case, charge transfer quenches full relaxation of the Pt−P bond, whereas in the Pd case the Pd−P bond length can increase more freely. Consequently, the emission of the Pt complexes is blue-shifted compared with that of the Pd complexes.

We note that in the study of Pt(II) complexes incorporating a pyridyl−acetylide ligand, it was recently found that N-protonation resulted in a blue shift of the absorption maxima and enhanced luminescence.[40]

CONCLUSION

The possibility of stabilizing tautomeric forms of functional diphosphine ligands by metal coordination has been demonstrated. Protonation of the nitrogen site of the oxazoline or pyridine moiety attached to the PCP carbon suggests that metal coordination at these positions should be accessible, which could lead to higher-nuclearity heterometallic structures. Whereas such investigations will be the subject of future work, preliminary experiments have shown that despite the isolobal analogy between H^+ and Au(I) reagents and their often similar bonding behavior,[41] the reaction of the Pd(II) analogue of **2b** with

dx.doi.org/10.1021/ic501566u | Inorg. Chem. 2014, 53, 12739−12756

Scheme 15. Comparison between the Sites of Reaction of the Anionic *P,P*-Chelating Diphosphino-oxazoline Ligand toward H^+ and a Au(I) Complex[3]

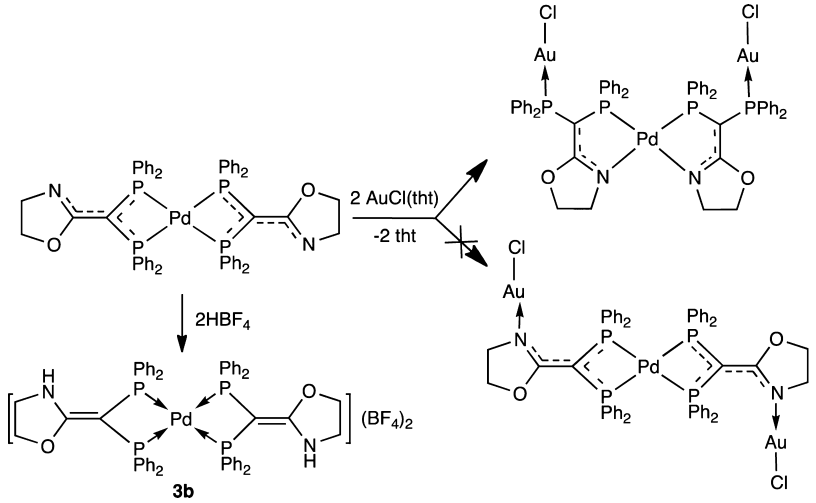

[AuCl(tht)] (tht = tetrahydrothiophene) did not result in gold coordination to the nitrogen site (as found for H^+ in **3b**) but rather to a change in the ligand coordination mode to palladium from *P,P*- to *P,N*-chelating while the second P donor was attached to the gold center (Scheme 15).[3] Clearly, the versatility of these functional ligands suggests that bonding rearrangements more complex than anticipated may occur in the course of their investigation.

Coordination of the free ligands to the metal cations completely changes the absorption spectra. The orbitals of the electron-rich ligands mix with empty orbitals of the cation to give a series of IL/LMCT states. The leaving orbitals are centered on the carbanion as in the free base and are more or less conjugated with the pyridine or oxazoline rings. The accepting orbitals change completely. Localized on the phenyls in the free base, after complexation they become a mixture of metal−phosphorus bonding/antibonding orbitals with some phenyl contributions. The lowest is issued from the last empty d orbital of the cation and the second-lowest from one of the empty p orbitals. The IL states are shifted far to the blue, and some metallic contribution remains.

The theoretical results have shown that the emitting state is a mixed LC/LMCT state derived from an antibonding orbital between the phosphorus and the metal cation with a small contribution from the cycle. This also explains the experimentally large Stokes shift, as the structure is significantly distorted upon excitation and the accepting orbital is relaxed. The changes in the emission properties arise from the metal orbital involved in the emission. This is the last empty d orbital, which is mixed with phosphorus lone pairs. The characteristics of the palladium 4d and platinum 5d orbitals explain the lower emission energy of the palladium complexes.

EXPERIMENTAL SECTION

General Considerations. All manipulations were carried out under an inert argon atmosphere using standard Schlenk line conditions. The solvents were dried and freshly distilled prior to use. Unless otherwise stated, the ^1H, $^{13}C\{^1H\}$, $^{31}P\{^1H\}$, and $^{19}F\{^1H\}$ NMR spectra were recorded on a Bruker Avance 300 instrument at 300.13, 75.47, 121.49, and 282.37 MHz, respectively, using TMS, H_3PO_4 (85% in D_2O), and $CFCl_3$ as external standards with downfield shifts reported as positive. All of the NMR spectra were measured at 298 K. The assignment of the signals was made by $^1H,^1H$-COSY, $^1H,^{13}C$-HMQC, and ^{13}C-HSQC experiments. Elemental C, H, and N analyses were performed by the Service de Microanalyses, Université de Strasbourg (France). Complexes $[PtCl_2(NCPh)_2]$,[42] **1**, and **2a** were prepared according to literature procedures. Ph_2PCl and NEt_3 were freshly distilled before use. Other chemicals were commercially available and were used as received.

Preparation and Spectroscopic Data for $[Pt(1')_2](BF_4)_2$ (3a). Aqueous HBF_4 (8.1 M, 1 mL, 8.1 mmol) was added to solid **2a** (0.200 g, 0.182 mmol), and the yellow solid became immediately colorless. After 10 min, this solid was washed with H_2O (3 × 20 mL) and acetone (3 × 5 mL), and the volatiles were removed under reduced pressure. Complex **3a** was isolated as a white powder. Yield: 0.216 g, 93% based on **2a**. Crystals suitable for X-ray diffraction were obtained by slow evaporation of a saturated CH_3CN solution. ^1H NMR (CD_3CN) δ 3.49 (t, 4H, ^3J(H,H) = 8.6 Hz, NCH_2), 4.34 (t, 4H, ^3J(H,H) = 8.6 Hz, OCH_2), 6.57 (br, 2H, NH), 7.28−7.48 (m, 40H, Ph); $^{31}P\{^1H\}$ NMR (CD_3CN) δ −34.4 (s with Pt satellites, ^1J(P,Pt) = 1989 Hz); $^{13}C\{^1H\}$ NMR (CD_3CN) δ 44.8 (s, NCH_2), 57.8 (t, ^1J(C,P) = 29.8 Hz, P−C−P), 71.3 (s, OCH_2), 130.3−133.9 (m, Ph), 171.1 (s with ^{195}Pt satellites, ^3J(C,Pt) = 86 Hz, O−*C*=N); $^{19}F\{^1H\}$ NMR δ −151.9 (s). Anal. Calcd (%) for **3a** (1275.59): C, 52.73; H, 3.95; N, 2.20. Found: C, 52.78; H, 4.30; N, 2.06.

Preparation and Spectroscopic Data for $[Pd(1')_2](BF_4)_2$ (3b). The procedure used for the preparation of **3a** was applied for **3b**, using 0.200 g (0.198 mmol) of solid **2b**. Complex **3b** was isolated as a very pale yellow solid. Yield: 0.221 g, 94%. ^1H NMR (CD_3CN) δ 3.54 (t, 4H, ^3J(H,H) = 8.7 Hz, NCH_2), 4.38 (t, 4H, ^3J(H,H) = 8.7 Hz, OCH_2), 6.62 (br, 2H, NH), 7.25−7.55 (m, 40H, Ph); $^{31}P\{^1H\}$ NMR (CD_3CN) δ −30.5 (br), −30.0 (br); $^{13}C\{^1H\}$ NMR (CD_3CN) δ 43.8 (s, NCH_2), 52.5 (t, ^1J(C,P) = 24.4 Hz, P−C−P), 70.3 (s, OCH_2), 129.4−132.8 (m, Ph), 167.7 (s); $^{19}F\{^1H\}$ NMR δ −151.9 (s). Anal. Calcd (%) for **3b** (1186.9): C, 56.67; H, 4.25; N, 2.36. Found: C, 56.45; H, 4.53; N, 2.28.

Preparation and Spectroscopic Data for [4-{Bis(diphenylphosphino)methyl}pyridine] (4). A solution of *n*-BuLi in hexane (19.3 mL, 1.6 M, 30.8 mmol) was added to a solution of 4-picoline (1.5 mL, 15.4 mmol) in THF (50 mL) over a period of 10 min at −78 °C. The mixture was stirred for 1 h, and PPh_2Cl (5.70 mL, 31.0 mmol) was added. The solution was allowed to reach room temperature under stirring. After evaporation of the volatiles under reduced pressure, the residue was dissolved in CH_2Cl_2 (40 mL). This solution was filtered, and the filtrate was evaporated to afford a yellow residue, which was washed with pentane (3 × 20 mL). Evaporation of the volatiles gave **4** as an off-white powder. Yield: 4.28 g, 60.1% based on 4-picoline. ^1H NMR ($CDCl_3$) δ 4.40 (s, 1H, PCHP), 6.78 (m, 2H, 2-Py), 7.14−7.47 (m, 20H, Ph), 8.11 (br, 2H, 3-Py); $^{31}P\{^1H\}$ NMR ($CDCl_3$) δ −3.3 (s); $^{13}C\{^1H\}$ NMR ($CDCl_3$) δ 44.2 (t, ^1J(C,P) = 28 Hz, P−C−P), 124.8 (br, 3-Py), 128.1−135.8 (m, Ph), 147.8 (s, 4-Py), 149.0

dx.doi.org/10.1021/ic501566u | *Inorg. Chem.* 2014, 53, 12739−12756

Table 9. X-ray Data Collection and Refinement Parameters

	3a	5a·2CH_3OH	6b·4CH_2Cl_2
chemical formula	$C_{56}H_{50}N_2O_2P_4Pt·2BF_4$	$C_{60}H_{48}N_2P_4Pt·2CH_4O$	$C_{60}H_{50}N_2P_4Pd·4CH_2Cl_2·2Cl$
formula mass	1275.57	1180.06	1439.90
crystal system	monoclinic	monoclinic	monoclinic
a (Å)	9.3583(3)	16.7379(6)	11.7472(5)
b (Å)	22.5243(8)	14.9479(7)	18.3989(8)
c (Å)	12.3493(2)	23.4480(6)	15.4885(6)
α (deg)	90.00	90.00	90.00
β (deg)	91.462(2)	109.125(2)	102.738(2)
γ (deg)	90.00	90.00	90.00
V (Å^3)	2602.25(13)	5542.8(4)	3265.2(2)
T (K)	173(2)	173(2)	173(2)
space group	$P21/c$	$C2/c$	$P21/c$
Z	2	4	2
μ (mm^{-1})	2.893	2.691	0.832
no. of reflections measured	18555	10911	12727
no. of independent reflections	6166	6343	7174
R_{int}	0.0862	0.0482	0.0489
final R_1 values ($I > 2\sigma(I)$)	0.0356	0.0430	0.0507
final $wR(F^2)$ values ($I > 2\sigma(I)$)	0.0818	0.0843	0.1236
final R_1 values (all data)	0.0609	0.0741	0.1013
final $wR(F^2)$ values (all data)	0.0918	0.0946	0.1443
goodness of fit on F^2	0.962	0.999	1.040

(s, 2-Py). Anal. Calcd (%) for **4** (461.47): C, 78.08; H, 5.46; N, 3.04. Found: C, 77.79; H, 5.68; N, 3.03.

Preparation and Spectroscopic Data for [Pt(4$_{-H}$)$_2$] (5a). Triethylamine (0.50 mL, 3.6 mmol) was added to a solution of **4** (0.530 g, 1.15 mmol) in acetonitrile (20 mL). After addition of [$PtCl_2$(NCPh)$_2$] (0.200 g, 0.42 mmol), the reaction mixture was stirred for 12 h, whereupon complex **5a** precipitated as a yellow solid. This solid was collected by filtration, washed with MeCN (3 × 5 mL), and dried under vacuum. Yield: 0.43 g, 90% based on Pt. Single crystals of **5a**·2CH_3OH suitable for X-ray analysis were obtained by slow evaporation of a saturated 1:1 CH_2Cl_2/CH_3OH solution. ^{1}H NMR (CD_2Cl_2) δ 6.31 (m, 4H, 3-Py), 7.12−7.44 (m, 40H, Ph), 7.68 (m, 4H, 2-Py); ^{31}P{^{1}H} NMR (CD_2Cl_2) δ −33.9 (s with Pt satellites, ^1J(P,Pt) = 1950 Hz); ^{13}C{^{1}H} NMR (CD_2Cl_2) δ 54.0 (tentative t masked by solvent peaks, ^1J(C,P) = 27 Hz, P−C−P), 116.0 (br, 3-Py), 128.4−132.6 (m, Ph), 147.0 (s, 2-Py), 153.7 (s, 4-Py). Anal. Calcd (%) for **5a**·CH_2Cl_2 (1199.19) (sample obtained by precipitation from a CH_2Cl_2 solution with pentane): C, 61.01; H, 4.20; N, 2.33. Found: C, 61.51; H, 4.44; N, 2.20 (no better C analysis could be obtained).

Preparation and Spectroscopic Data for [Pd(4$_{-H}$)$_2$] (5b). Solid [Pd(acac)$_2$] (0.095 g, 0.31 mmol) was added to a stirred solution of **4** (0.30 g, 0.65 mmol) in CH_2Cl_2 (20 mL). The reaction mixture was stirred for 12 h, during which an orange solid precipitated. The volatiles were removed under reduced pressure, and the orange residue was washed with THF (3 × 10 mL) and dried under vacuum, giving **5b** as an orange solid. The complex was further purified by precipitation from CH_2Cl_2/pentane. Yield: 0.29 g, 91% based on Pd. ^{1}H NMR ($CDCl_3$) δ 6.33 (m, 4H, 3-Py), 7.11−7.34 (m, 40H, Ph), 7.70 (br, 4H, 2-Py); ^{31}P{^{1}H} NMR ($CDCl_3$) δ −29.4 (s); ^{13}C{^{1}H} NMR ($CDCl_3$) δ 53.6 (tentative br, P−C−P), 116.3 (s, 3-Py), 128.7−132.5 (m, Ph), 146.1 (br, 2-Py), 152.0 (s, 4-Py). Anal. Calcd (%) for **5b**·3CH_2Cl_2 (1282.15): C, 59.02; H, 4.25; N, 2.18. Found: C, 59.29; H, 4.30; N, 2.17.

Preparation and Spectroscopic Data for (5a·2HCl) (6a). Solid [$PtCl_2$(NCPh)$_2$] (0.100 g, 0.21 mmol) was added to a stirred solution of **4** (0.210 g, 0.4 mmol) in THF (20 mL). The reaction mixture was stirred for 2 h, during which complex **6a** precipitated as a pale-yellow solid. It was collected by filtration, washed with diethyl ether (3 × 10 mL), and dried under vacuum. Yield: 0.24 g, 95% based on Pt. ^{1}H NMR (CD_3OD) δ 6.45 (m, 4H, 3-Py), 7.23−7.49 (m, 40H, Ph), 7.48 (masked by the Ph signals, observed by ^{1}H,^{1}H-COSY and ^{1}H,^{13}C-HMQC, 4H, 2-Py); ^{31}P{^{1}H} NMR (CD_3OD) δ −31.4 (s with Pt satellites, ^1J(P,Pt) = 1975 Hz); ^{13}C{^{1}H} NMR (CD_3OD) δ 53.7 (tentative br, P−C−P), 116.0 (br, 3-Py), 128.6−134.1 (m, Ph), 137.4 (br, 2-Py), 151.8 (s, 4-Py). Anal. Calcd (%) for **6a** (1188.93): C, 60.61; H, 4.24; N, 2.36. Found: C, 60.62; H, 4.27; N, 2.20.

Preparation and Spectroscopic Data for (5b·2HCl) (6b). The procedure described for complex **6a** was also applied to the synthesis of **6b**, using [$PdCl_2$(NCPh)$_2$] (0.100 g, 0.26 mmol) and **4** (0.260 g, 0.56 mmol). Yield: 0.27 g, 94% based on Pd. Crystals suitable for X-ray diffraction were obtained by slow evaporation of a saturated CH_2Cl_2/CH_3CN solution. ^{1}H NMR (CD_2Cl_2) δ 6.34 (m, 4H, 3-Py), 7.15−7.44 (m, 40H, Ph), 7.41 (masked by the Ph signals, observed by ^{1}H,^{1}H-COSY and ^{1}H,^{13}C-HMQC, 4H, 2-Py); ^{31}P{^{1}H} NMR ($CDCl_3$) δ −28.5 (s); ^{13}C{^{1}H} NMR ($CDCl_3$) δ 53.7 (tentative t masked by solvent peaks, ^1J(C,P) = 27 Hz, P−C−P), 115.2 (br, 3-Py), 129.0−132.6 (m, Ph), 136.1 (br, 2-Py), 158.3 (s, 4-Py). Anal. Calcd (%) for **6b**·0.5CH_2Cl_2 (1142.73): C, 63.59; H, 4.50; N, 2.45. Found: C, 63.10; H, 4.84; N, 2.23.

X-ray Data Collection, Structure Solution, and Refinement for All Compounds. Crystals suitable for the X-ray analysis of each compound were obtained as described above. The intensity data were collected on a Kappa CCD diffractometer[43] using graphite-monochromatized Mo Kα radiation (λ = 0.71073 Å) at 173(2) K. Crystallographic and experimental details for the structures are summarized in Table 9. The structures were solved by direct methods (SHELXS-97) and refined by full-matrix least-squares procedures based on F^2 (SHELXL-97)[44] with anisotropic thermal parameters for all of the non-hydrogen atoms. Hydrogen atoms were introduced into the geometrically calculated positions (SHELXL-97 procedures) and refined riding on the corresponding parent atoms.

Photophysical Studies. *Absorption Spectroscopy.* Absorption spectra were measured using a Varian Cary 5000 double-beam UV−vis−NIR spectrometer and baseline-corrected.

Emission Spectroscopy. Steady-state emission spectra were recorded on a HORIBA Jobin-Yvon IBH FL-322 Fluorolog 3 spectrometer equipped with a 450 W xenon arc lamp, double-grating excitation and emission monochromators (2.1 nm mm^{-1}; 1200 grooves mm^{-1}), and a TBX-04 detector. Emission and excitation spectra were corrected for source intensity (lamp and grating) and emission spectral response (detector and grating) using standard correction curves. Time-resolved measurements were performed using the time-correlated single-photon counting (TCSPC) option on the Fluorolog 3. NanoLEDs

(430 nm, fwhm <200 ps or 402 nm, fwhm <750 ps) with repetition rates between 10 kHz and 1 MHz were used to excite the sample. The excitation source was mounted on the sample chamber at an angle of 90° to a double-grating emission monochromator (2.1 nm mm^{-1} dispersion, 1200 grooves mm^{-1}) and collected using a TBX-04 single-photon-counting detector. The photons collected at the detector were correlated to the excitation pulse using a time-to-amplitude converter. Signals were collected using an IBH DataStation Hub photon counting module, and data analysis was performed using the commercially available DAS6 software (HORIBA Jobin Yvon IBH). The goodness of fit was assessed by minimizing the reduced χ^2 function and visual inspection of the weighted residuals. All of the reported fittings showed χ^2 values in the range 0.95−1.2. Emission lifetimes greater than 10 μs were recorded on the same fluorimeter using a microsecond Xe flash and MCS electronic option. The PLQYs of solid-state samples, both powders and thin films, were recorded at a fixed excitation wavelength using a Hamamatsu Photonics absolute PLQY measurement system (C9920-02) equipped with an L9700-01 continuous-wave xenon light source (150 W), monochromator, integrating sphere, and C7473 photonics multichannel analyzer and employing the commercially available U6039-05 PLQY measurement software (Hamamatsu Photonics Ltd., Shizuoka, Japan). All of the solvents used for the photophysical measurements were spectroscopic grade.

Thin-Film Sample Preparation. Thin films for spectroscopic measurements were prepared from 5 wt % solutions of PMMA (MW = 35 000) in CH_2Cl_2 (spectroscopic grade) and spun onto quartz substrates using a 2000 rpm spin cycle. All of the samples were then treated to dynamic vacuum to remove incorporated solvent. For the experiments involving the addition of TFA to the complexes, concentrated stock solutions of TFA in DMF were added dropwise directly to the cuvettes of ready-to-measure samples. During the measurement time all of the complexes studied were stable in solution, as demonstrated by the lack of change in the absorption spectrum before and after the measurements. PMMA was purchased from Aldrich.

Computational Details. The molecular structures of **2a**, **2b**, **5a**, and **5b** reported in Tables S2−S6 in the Supporting Information, the formulas of which are depicted in Figure 4, were optimized in the gas phase by DFT with the ADF package[45] using the B3LYP functional[46] with all electrons and triple-ζ basis sets.[47] The scalar relativistic effects were taken into account within the zero-order regular approximation (ZORA).[48]

The nature of the stationary state was checked through a complete set of real frequencies. The Pd and Pt PCP-oxazoline complexes **2a** and **2b** depicted in Figure 4 possess a center of inversion on the cation and belong to the C_i symmetry group. The platinum complex with the pyridine derivatives converges to C_2 symmetry according to the frequency analysis.

The energies of transitions to the low-lying singlet excited states were computed by means of TD-DFT[49] (B3LYP) calculations in the gas phase. Solvent corrections were added for complexes **2b** and **5b** in order to check the validity of the gas-phase results. The transition energies were not affected by this correction, in line with the absence of observed solvatochromism in the molecules under investigation. The analysis of the theoretical absorption spectra was based on electron density differences computed from Kohn−Sham orbitals and their occupations in the electronic ground state and excited states. This work was done using the DGRID package from Kohout.[50]

In order to interpret the emission spectra, the geometries of the electronic excited states of interest should have been optimized at the TD-DFT level for the lowest triplet and singlet states according to the strategy applied recently with success to square-planar Pt(II) emissive complexes.[51] However, our tentative attempts failed because of severe convergence problems for the singlet states. Consequently, the emission spectra of the complexes were constructed from TD-DFT calculations performed on the triplet excited-state geometries. This method is justified by the very similar geometries we obtained for the singlet and associated triplet states in the case of square-planar Pt(II) complexes with bidentate and tridentate ligands.[51] Solvent corrections were taken into account through the polarizable continuum model (PCM)[52] for DMF (ε = 37.219).

■ ASSOCIATED CONTENT

Supporting Information

Listings of emission spectra and theoretical data, absorption spectra and electronic densities, and X-ray data (CIF). This material is available free of charge via the Internet at http://pubs.acs.org. CCDC 964885−964887 contain the supplementary crystallographic data for this paper. These data can be obtained free of charge from the Cambridge Crystallographic Data Center via www.ccdc.cam.ac.uk/data_request/cif.

■ AUTHOR INFORMATION

Corresponding Authors

*Tel: +33 (0)3 68 85 13 08. braunstein@unistra.fr.
*Tel:+33 (0)3 68 85 52 20. Fax:+33 (0)3 68 85 52 42. decola@unistra.fr.
*Tel: +33 (0)3 68 85 13 14. c.daniel@unistra.fr.

Notes

The authors declare no competing financial interest.

■ ACKNOWLEDGMENTS

The work was supported by the CNRS, the Ministère de l'Enseignement Supérieur et de la Recherche, and the Agence Nationale de la Recherche (ANR-06-BLAN 410). The authors are grateful to Dr. K. Yu. Monakhov and thank Lionel Allouche for NMR experiments. The calculations were performed at the High Performance Computing Centre (HPC, unistra).

■ REFERENCES

(1) For example, see: (a) Slone, C. S.; Weinberger, D. A.; Mirkin, C. A. *Prog. Inorg. Chem.* **1999**, *48*, 233−350. (b) Espinet, P.; Soulantica, K. *Coord. Chem. Rev.* **1999**, *193*−*195*, 499−556. (c) Helmchen, G.; Pfaltz, A. *Acc. Chem. Res.* **2000**, *33*, 336−345. (d) Chelucci, G.; Orru, G.; Pinna, G. A. *Tetrahedron* **2003**, *59*, 9471−9515. (e) Rechavi, D.; Lemaire, M. *Chem. Rev.* **2002**, *102*, 3467−3493. (f) Pfaltz, A.; Blankenstein, J.; Hilgraf, R.; Hormann, E.; McIntyre, S.; Menges, F.; Schonleber, M.; Smidt, S. P.; Wustenberg, B.; Zimmermann, N. *Adv. Synth. Catal.* **2003**, *345*, 33−44. (g) McManus, H. A.; Guiry, P. J. *Chem. Rev.* **2004**, *104*, 4151. (h) Guiry, P. J.; Saunders, C. P. *Adv. Synth. Catal.* **2004**, *346*, 497−537. (i) Desimoni, G.; Faita, G.; Jørgensen, K. A. *Chem. Rev.* **2006**, *106*, 3561−3651. (j) Roseblade, S. J.; Pfaltz, A. *Acc. Chem. Res.* **2007**, *40*, 1402−1411. (k) Hou, J.; Sun, W.-H.; Zhang, S.; Ma, H.; Deng, Y.; Lu, X. *Organometallics* **2006**, *25*, 236−244. (l) Benito-Garagorri, D.; Kirchner, K. *Acc. Chem. Res.* **2008**, *41*, 201−213. (m) Maggini, S. *Coord. Chem. Rev.* **2009**, *253*, 1793−1832. (n) Mata, Y.; Pamies, O.; Dieguez, M. *Adv. Synth. Catal.* **2009**, *351*, 3217−3234. (o) Willms, H.; Frank, W.; Ganter, C. *Organometallics* **2009**, *28*, 3049−3058. (p) Flapper, J.; Kooijman, H.; Lutz, M.; Spek, A. L.; van Leeuwen, P. W. N. M.; Elsevier, C. J.; Kamer, P. C. J. *Organometallics* **2009**, *28*, 3272−3281.

(2) (a) Braunstein, P.; Naud, F. *Angew. Chem., Int. Ed.* **2001**, *40*, 680−699. (b) Wingerter, S.; Pfeiffer, M.; Murso, A.; Lustig, C.; Stey, T.; Chandrasekhar, V.; Stalke, D. *J. Am. Chem. Soc.* **2001**, *123*, 1381−1388. (c) Braunstein, P.; Clerc, G.; Morise, X.; Welter, R.; Mantovani, G. *Dalton Trans.* **2003**, 1601−1605. (d) Oberbeckmann-Winter, N.; Braunstein, P.; Welter, R. *Organometallics* **2004**, *23*, 6311−6318. (e) Murso, A.; Stalke, D. *Dalton Trans.* **2004**, 2563−2569. (f) Braunstein, P. *J. Organomet. Chem.* **2004**, *689*, 3953−3967. (g) Speiser, F.; Braunstein, P.; Saussine, L. *Acc. Chem. Res.* **2005**, *38*, 784−793. (h) Braunstein, P. *Chem. Rev.* **2006**, *106*, 134−159. (i) Kermagoret, A.; Pattacini, R.; Chavez, V. P.; Rogez, G.; Welter, R.; Braunstein, P. *Angew. Chem., Int. Ed.* **2007**, *46*, 6438−6441. (j) Agostinho, M.; Braunstein, P. *Chem. Commun.* **2007**, 58−60. (k) Agostinho, M.; Braunstein, P. *C. R. Chim.* **2007**, *10*, 666−676. (l) Jie, S.; Agostinho, M.; Kermagoret, A.; Cazin, C. S. J.; Braunstein, P. *Dalton Trans.* **2007**, 4472−4482. (m) Kermagoret, A.; Braunstein, P. *Organometallics* **2008**, *27*, 88−99. (n) Kermagoret, A.; Braunstein, P.

Dalton Trans. **2008**, 585−587. (o) Kermagoret, A.; Tomicki, F.; Braunstein, P. *Dalton Trans.* **2008**, 2945−2955. (p) Pattacini, R.; Jie, S.; Braunstein, P. *Chem. Commun.* **2009**, 890−892. (q) Chavez, P.; Guerrero Rios, I.; Kermagoret, A.; Pattacini, R.; Meli, A.; Bianchini, C.; Giambastiani, G.; Braunstein, P. *Organometallics* **2009**, *28*, 1776−1784. (r) O'Reilly, M.; Pattacini, R.; Braunstein, P. *Dalton Trans.* **2009**, 6092−6095. (s) Peloso, R.; Pattacini, R.; Cazin, C. S. J.; Braunstein, P. *Inorg. Chem.* **2009**, *48*, 11415−11424. (t) Zhang, J.; Pattacini, R.; Braunstein, P. *Inorg. Chem.* **2009**, *48*, 11954−11962. (u) Liu, S.; Peloso, R.; Braunstein, P. *Dalton Trans.* **2010**, *39*, 2563−2572. (v) Zhang, S.; Pattacini, R.; Braunstein, P. *Organometallics* **2010**, *29*, 6660−6667. (w) Zhang, S.; Pattacini, R.; Jie, S.; Braunstein, P. *Dalton Trans.* **2012**, *41*, 379−386. (x) Zhang, S.; Pattacini, R.; Braunstein, P. *Dalton Trans.* **2011**, *40*, 5711−5719. (y) Liu, S.; Pattacini, R.; Braunstein, P. *Organometallics* **2011**, *30*, 3549−3558. (z) Zhang, S.; Pattacini, R.; Jie, S.; Braunstein, P. *Dalton Trans.* **2012**, *41*, 379−386. (aa) Zhang, S.; Pattacini, R.; Braunstein, P. Coordination Chemistry of Oxazoline/Thiazoline-Based P,N Ligands. In *Advances in Organometallic Chemistry: The Silver/Gold Jubilee International Conference on Organometallic Chemistry Celebratory Book*; Pombeiro, A. J. L., Ed.; John Wiley & Sons: Hoboken, NJ, 2014; Chapter 14, pp 185−198 and references cited therein.

(3) Zhang, S.; Pattacini, R.; Braunstein, P. *Inorg. Chem.* **2011**, *50*, 3511−3522.

(4) Pattacini, R.; Margraf, G.; Messaoudi, A.; Oberbeckmann-Winter, N.; Braunstein, P. *Inorg. Chem.* **2008**, *47*, 9886−9897.

(5) For example, see: (a) Puddephatt, R. J. *Chem. Soc. Rev.* **1983**, *12*, 99−127. (b) Braunstein, P. *Mater. Chem. Phys.* **1991**, *29*, 33−63. (c) Balakrishna, M. S.; Reddy, V. S.; Krishnamurthy, S. S.; Nixon, J. F.; St. Laurent, J. C. T. R. B. *Coord. Chem. Rev.* **1994**, *129*, 1−90. (d) Braunstein, P. *New J. Chem.* **1994**, *18*, 51−60. (e) Bhattacharyya, P.; Woolins, J. D. *Polyhedron* **1995**, *14*, 3367−3388. (f) Mague, J. T. *J. Cluster Sci.* **1995**, *6*, 217−269. (g) Rodriguez-Zubiri, M.; Gallo, V.; Rosé, J.; Welter, R.; Braunstein, P. *Chem. Commun.* **2008**, 64−66. (h) Fliedel, C.; Pattacini, R.; Braunstein, P. *J. Clust. Sci.* **2010**, *21*, 397−415. (i) Rosa, R.; Fliedel, C.; Ghisolfi, A.; Pattacini, R.; Avilés, T.; Braunstein, P. *Dalton Trans.* **2013**, *42*, 12109−12119.

(6) (a) Braunstein, P.; Kormann, H.-P.; Meyer-Zaika, W.; Pugin, R.; Schmid, G. *Chem.—Eur. J.* **2000**, *6*, 4637−4646. (b) Schweyer-Tihay, F.; Braunstein, P.; Estournès, C.; Guille, J. L.; Lebeau, B.; Paillaud, J.-L.; Richard-Plouet, M.; Rosé, J. *Chem. Mater.* **2003**, *15*, 57−62. (c) Braunstein, P. *J. Organomet. Chem.* **2004**, *689*, 3953−3967.

(7) Mague, J. T.; Krinsky, J. L. *Inorg. Chem.* **2001**, *40*, 1962−1971.

(8) Anderson, M. P.; Mattson, B. M.; Pignolet, L. H. *Inorg. Chem.* **1983**, *22*, 2644−2647.

(9) (a) Anderson, M. P.; Pignolet, L. H. *Organometallics* **1983**, *2*, 1246−1247. (b) Anderson, M. P.; Tso, C. C.; Mattson, B. M.; Pignolet, L. H. *Inorg. Chem.* **1983**, *22*, 3267−3275. (c) McNair, R. J.; Nilsson, P. V.; Pignolet, L. H. *Inorg. Chem.* **1985**, *24*, 1935−1939. (d) McNair, R. J.; Pignolet, L. H. *Inorg. Chem.* **1986**, *25*, 4717−4723. (e) Mattson, B. M.; Ito, L. N. *Organometallics* **1989**, *8*, 391−395. (f) Mague, J. T.; Hawbaker, S. W. *J. Chem. Crystallogr.* **1997**, *27*, 603−608. (g) Lang, H.-F.; Fanwick, P. E.; Walton, R. A. *Inorg. Chim. Acta* **2002**, *328*, 232−236.

(10) For example, see: (a) Kato, M.; Omura, A.; Toshikawa, A.; Kishi, S.; Sugimoto, Y. *Angew. Chem., Int. Ed.* **2002**, *41*, 3183−3185. (b) Kato, M. *Bull. Chem. Soc. Jpn.* **2007**, *80*, 287−294. (c) Drew, S. M.; Janzen, D. E.; Buss, C. E.; MacEwan, D. I.; Dublin, K. M.; Mann, K. R. *J. Am. Chem. Soc.* **2001**, *123*, 8418−8420. (d) Grove, L. J.; Rennekamp, J. M.; Jude, H.; Connick, W. B. *J. Am. Chem. Soc.* **2004**, *126*, 1594−1595. (e) Wadas, T. J.; Wang, Q.-M.; Kim, Y. J.; Flaschenreim, C.; Blaton, T. N.; Eisenberg, R. *J. Am. Chem. Soc.* **2004**, *126*, 16841−16849. (f) Mastuzaki, H.; Kishida, H.; Okamoto, H.; Takizawa, K.; Matsunaga, S.; Takaishi, S.; Miyasaka, H.; Sugiura, K.; Yamashita, M. *Angew. Chem., Int. Ed.* **2005**, *44*, 3240−3243. (g) Kui, S. C. F.; Chui, S. S.-Y.; Che, C.-M.; Zhu, N. *J. Am. Chem. Soc.* **2006**, *128*, 8297−8309. (h) Muro, M. L.; Daws, C. A.; Castellano, F. N. *Chem. Commun.* **2008**, 6134−6136. (i) Du, P.; Schneider, J.; Brennessel, W. W.; Eisenberg, R. *Inorg. Chem.* **2008**, *47*, 69−77. (j) Mathew, I.; Li, Y.; Li, Z.; Sun, W. *Dalton Trans.* **2010**, *39*, 11201−11209. (k) Hudson, Z. M.; Sun, C.; Harris, K. J.; Lucier, B. E. G.; Schurko, R. W.; Wang, S. *Inorg. Chem.* **2011**, *50*, 3447−3457. (l) Kobayashi, A.; Fukuzawa, Y.; Chang, H.-C.; Kato, M. *Inorg. Chem.* **2012**, *51*, 7508−7519. (m) Ohba, T.; Kobayashi, A.; Chang, H.-C.; Kato, M. *Dalton Trans.* **2013**, *42*, 5514−5523.

(11) (a) Cebrián, C.; Mauro, M.; Kourkoulos, D.; Mercandelli, P.; Hertel, D.; Meerholz, K.; Strassert, C. A.; De Cola, L. *Adv. Mater.* **2013**, *25*, 437−442. (b) Mydlak, M.; Mauro, M.; Polo, F.; Felicetti, M.; Leonhardt, J.; Diener, G.; De Cola, L.; Strassert, C. A. *Chem. Mater.* **2011**, *23*, 3659−3667. (c) Strassert, C. A.; Chien, C.-H.; Galvez Lopez, M. D.; Kourkoulos, D.; Hertel, D.; Meerholz, K.; De Cola, L. *Angew. Chem., Int. Ed.* **2011**, *50*, 946−950. (d) Borek, C.; Hanson, K.; Djurovich, P. I.; Thompson, M. E.; Aznavour, K.; Bau, R.; Sun, Y.; Forrest, S. R.; Brooks, J.; Michalski, L.; Brown, J. *Angew. Chem., Int. Ed.* **2007**, *46*, 1109−1112. (e) Li, K.; Guan, X.; Ma, C.-W.; Lu, W.; Chen, Y.; Che, C.-M. *Chem. Commun.* **2011**, *47*, 9075−9077. (f) Meyer, A.; Unger, Y.; Poethig, A.; Strassner, T. *Organometallics* **2011**, *30*, 2980−2985. (g) Mróz, W.; Botta, C.; Giovanella, U.; Rossi, E.; Colombo, A.; Dragonetti, C.; Roberto, D.; Ugo, R.; Valore, A.; Williams, J. A. G. *J. Mater. Chem.* **2011**, *21*, 8653−8661. (h) Ma, B.; Djurovich, P. I.; Garon, S.; Alleyne, B.; Thompson, M. E. *Adv. Mater.* **2006**, *16*, 2438−2446. For some recent reviews, see: (j) Kalinowski, J.; Fattori, V.; Cocchi, M.; Williams, J. A. G. *Coord. Chem. Rev.* **2011**, *255*, 2401−2425. (k) Williams, J. A. G.; Develay, S.; Rochester, D. L.; Murphy, L. *Coord. Chem. Rev.* **2008**, *252*, 2596−2611. (l) Murphy, L. In *Highly Efficient OLEDs with Phosphorescent Materials*; Yersin, H., Ed.; Wiley-VCH: Weinheim, Germany, 2008. (m) Thompson, M. E.; Djurovich, P. E.; Barlow, S.; Marder, S. Organometallic Complexes for Optoelectronic Applications. In *Comprehensive Organometallic Chemistry III*; Crabtree, R. H., Mingos, D. M. P., Eds.; Elsevier: Oxford, U.K., 2006.

(12) For example, see: Diez, A.; Fornies, J.; Garcia, A.; Lalinde, E.; Moreno, M. T. *Inorg. Chem.* **2005**, *44*, 2443−2453.

(13) For example, see: Bridgeman, A. J.; Gerloch, M. *J. Chem. Soc., Dalton Trans.* **1995**, 197−204.

(14) For recent examples, see: (a) Leung, S. Y.-L.; Lam, W. H.; Zhu, N.; Yam, V. W.-W. *Organometallics* **2010**, *29*, 5558−5569. (b) Morley, C. P.; Webster, C. A.; Douglas, P.; Rofe, K.; Di Vaira, M. *Dalton Trans.* **2010**, *39*, 3177−3189. (c) Bellows, D.; Goudreault, T.; Aly, S. M.; Fortin, D.; Gros, C. P.; Barbe, J.-M.; Harvey, P. D. *Organometallics* **2010**, *29*, 317−325. (d) Clément, S.; Aly, S. M.; Husson, J.; Fortin, D.; Strohmann, C.; Knorr, M.; Guyard, L.; Abd-El-Aziz, A. S.; Harvey, P. D. *Eur. J. Inorg. Chem.* **2009**, 2536−2546. (e) Clement, S.; Aly, S. M.; Bellows, D.; Fortin, D.; Strohmann, C.; Guyard, L.; Abd-El-Aziz, A. S.; Knorr, M.; Harvey, P. D. *Inorg. Chem.* **2009**, *48*, 4118−4133. (f) Bellows, D.; Gingras, E.; Aly, S. M.; Abd-El-Aziz, A. S.; Leclerc, M.; Harvey, P. D. *Inorg. Chem.* **2008**, *47*, 11720−11733. (g) Clement, S.; Mohammed, A. S.; Fortin, D.; Guyard, L.; Knorr, M.; Abd-El-Aziz, A. S.; Harvey, P. D. *Inorg. Chem.* **2008**, *47*, 10816−10824. (h) Ding, J.; Pan, D.; Tung, C.-H.; Wu, L.-Z. *Inorg. Chem.* **2008**, *47*, 5099−5106. (i) Kui, S. C. F.; Sham, I. H. T.; Cheung, C. C. C.; Ma, H.-W.; Yan, B.; Zhu, N.; Che, C.-M.; Fu, W.-F. *Chem.—Eur. J.* **2007**, *13*, 417−435. (j) Xu, H.-B.; Zhang, L.-Y.; Chen, Z.-N. *Inorg. Chim. Acta* **2007**, *360*, 163−169.

(15) Pickaert, G.; Douce, L.; Ziessel, R.; Cesario, M. *Chem. Commun.* **2000**, 1125−1126.

(16) (a) Nelson, S. M.; Perks, M.; Walker, B. J. *J. Chem. Soc., Perkin Trans. 1* **1976**, 1205−1209. (b) Dahlhoff, W. V.; Dick, T. R.; Ford, G. H.; Kelly, W. S. J.; Nelson, S. M. *J. Chem. Soc. A* **1971**, *22*, 3495−3499.

(17) (a) Favez, R.; Roulet, R.; Pinkerton, A. A.; Schwarzenbach, D. *Inorg. Chem.* **1980**, *19*, 1356−1365. (b) Pregosin, P. S. In *Phosphorus-31 NMR Spectroscopy in Stereochemical Analysis*; VCH Publishers: Weinheim, Germany, 1987.

(18) Lang, H.-F.; Fanwick, P. E.; Walton, R. A. *Inorg. Chim. Acta* **2002**, *328*, 232−236.

(19) Gero, A.; Markham, J. J. *J. Org. Chem.* **1951**, *16*, 1835−1838.

(20) Chen, I. J.; MacKerell, A. D., Jr. *Theor. Chem. Acc.* **2000**, *103*, 483−494.

(21) Park, Y. J.; Sickerman, N. S.; Ziller, J. W.; Borovik, A. S. *Chem. Commun.* **2007**, *46*, 2584−2586.

(22) Pattacini, R.; Giansante, C.; Ceroni, P.; Maestri, M.; Braunstein, P. *Chem.—Eur. J.* **2007**, *13*, 10117−10128.

(23) Hamada, A.; Braunstein, P. *Inorg. Chem.* **2009**, *48*, 1624−1637.
(24) Maestri, M.; Deuschel-Cornioley, C.; von Zelewsky, A. *Coord. Chem. Rev.* **1991**, *111*, 117−123.
(25) van der Ploeg, A. F. M. J.; van Koten, G.; Schitz, J. E. J.; van der Linden, J. G. M. *Inorg. Chim. Acta* **1982**, *58*, 53−58.
(26) Grey, J. K.; Butler, I. S.; Reber, C. *Inorg. Chem.* **2003**, *42*, 6503−6518.
(27) Pelletier, Y.; Reber, C. *Inorg. Chem.* **1997**, *36*, 721−728.
(28) Genre, C.; Levasseur-Theriault, G.; Reber, C. *Can. J. Chem.* **2009**, *87*, 1625−1635.
(29) Jude, H.; Bauer, J. A. K.; Connick, W. B. *Inorg. Chem.* **2002**, *41*, 2275−2281.
(30) Barigelletti, F.; Sandrini, D.; Maestri, M.; Balzani, V.; von Zelewsky, A.; Chassot, L.; Jolliet, P.; Maeder, U. *Inorg. Chem.* **1988**, *27*, 3644−3647.
(31) Maestri, M.; Sandrini, D.; Balzani, V.; von Zelewsky, A.; Deuschel-Cornioley, C.; Jolliet, P. *Helv. Chim. Acta* **1988**, *71*, 1053−1059.
(32) Puzyk, M. V.; Ivanov, M. A.; Balashev, K. P. *Opt. Spectrosc.* **2003**, *95*, 581−584.
(33) Van der Ploeg, A. F. M. J.; Van Koten, G.; Schmitz, J. E. J.; Van der Linden, J. G. M. *Inorg. Chim. Acta* **1982**, *58*, 53−58.
(34) Quartapelle Procopio, E.; Mauro, M.; Panigati, M.; Donghi, D.; Mercandelli, P.; Sironi, A.; D'Alfonso, G.; De Cola, L. *J. Am. Chem. Soc.* **2010**, *132*, 14397−14399.
(35) Talarico, A. M.; Aiello, I.; Bellusci, A.; Crispini, A.; Ghedini, M.; Godbert, N.; Pugliese, T.; Szerb, E. *Dalton Trans.* **2010**, *39*, 1709−1712.
(36) Field, J. S.; Ledwaba, L. P.; Munro, O. Q.; McMillin, D. R. *CrystEngComm* **2008**, *10*, 740−747.
(37) Yam, W. W. W.; Wong, K. M.-C.; Zhu, N. *J. Am. Chem. Soc.* **2002**, *124*, 6506−6507.
(38) Brinkmann, M.; Gadret, G.; Muccini, M.; Taliani, C.; Masciocchi, N.; Sironi, A. *J. Am. Chem. Soc.* **2000**, *122*, 5147−5157.
(39) Desclaux, J. P. *At. Data Nucl. Data Tables* **1973**, *12*, 311−406.
(40) Latouche, C.; Lanoë, P.-H.; Williams, J. A. G.; Guerchais, V.; Boucekkine, A.; Fillaut, J.-L. *New J. Chem.* **2011**, *35*, 2196−2202.
(41) (a) Hoffmann, R. *Angew. Chem., Int. Ed. Engl.* **1982**, *21*, 711−724. (b) Mingos, D. M. P. *Gold Bull.* **1984**, *17*, 5−12. (c) Braunstein, P.; Rosé, J. *Gold Bull.* **1985**, *18*, 17−30.
(42) (a) Hartley, F. R. *The Chemistry of Platinum and Palladium*; Applied Science Publishers: London, 1973. (b) Braunstein, P.; Bender, R.; Jud, J. *Inorg. Synth.* **1989**, *26*, 341−350.
(43) *Kappa CCD Reference Manual*; Nonius BV: The Netherlands, 1998.
(44) Sheldrick, G. M. *Acta Crystallogr.* **2008**, *A64*, 112−122.
(45) *ADF 2012*; Scientific Computing & Modelling NV: Amsterdam, 2014; http://www.scm.com.
(46) Stephens, P. J.; Devlin, F. J.; Chabalowski, C. F.; Frisch, M. J. *J. Phys. Chem.* **1994**, *98*, 11623−11627.
(47) van Lenthe, E.; Baerends, E. J. *J. Comput. Chem.* **2003**, *24*, 1142−1156.
(48) van Lenthe, E.; van Leeuwen, R.; Baerends, E. J.; Snijders, J. G. *Int. J. Quantum Chem.* **1996**, *57*, 281−293.
(49) Rosa, A.; Baerends, E. J.; van Gisbergen, S. J. A.; van Lenthe, E.; Groeneveld, J. A.; Snijders, J. G. *J. Am. Chem. Soc.* **1999**, *121*, 10356−10365.
(50) Kohout, M. *DGrid*, version 4.5; Radebeul, Germany, 2009.
(51) Gourlaouen, C.; Daniel, C. *Dalton Trans.* **2014**, DOI: 10.1039/c4dt01822b.
(52) Pye, C. C.; Ziegler, T. *Theor. Chem. Acc.* **1999**, *101*, 396−408.